Label-free biosensor of phagocytosis for diagnosing bacterial infections

Junchen Liao, Jifeng Ren, Raymond H. W. Lam, Song Lin Chua, Bee Luan Khoo**

J. Liao, J. Ren, Prof R. H. W. Lam, Prof. B L Khoo
Department of Biomedical Engineering
City University of Hong Kong,
Hong Kong SAR, China
E-mail: blkhoo@cityu.edu.hk

J. Ren
School of Biomedical Engineering
Capital Medical University
Beijing 100069, China

Prof R. H. W. Lam
City University of Hong Kong Shenzhen Research Institute
Shenzhen 518057, China
Centre for Robotics and Automation
City University of Hong Kong
Hong Kong SAR, China

Prof S. L. Chua
Department of Applied Biology and Chemical Technology
The Hong Kong Polytechnic University
Hong Kong SAR 999077, China
State Key Laboratory of Chemical Biology and Drug Discovery
The Hong Kong Polytechnic University
Hong Kong SAR 999077, China
Shenzhen Key Laboratory of Food Biological Safety Control
E-mail: song-lin.chua@polyu.edu.hk

Keywords: Phagocytosis; Microfluidics; Infections; Diagnosis

Abstract

Phagocytic cells recognize and phagocytose invading microbes for destruction. However, bacterial pathogens can remain hidden at low levels from conventional detection or replicate intracellularly after being phagocytosed by immune cells. Current phagocytosis-detection approaches involve flow cytometry or microscopic search for rare bacteria-internalized phagocytes among large populations of uninfected cells, which poses significant challenges in research and clinical settings. Hence it is imperative to develop a rapid, non-disruptive, and label-free phagocytosis detection approach. Using deformability assays and microscopic imaging, we revealed that phagocytosis led to aberrant physical properties in monocytes. Specifically, human monocytes with internalized bacteria of various species were stiffer and larger compared with uninfected monocytes. Taking advantage of these physical differences, a novel microfluidics-based biosensor platform was developed to passively sort, concentrate and quantify rare monocytes with internalized pathogens (MIP) from uninfected monocyte populations for phagocytosis detection. The clinical utility of the MIP platform was demonstrated by enriching and detecting bacteria-internalized monocytes from spiked human blood samples within 1.5 h. Patient clinical isolates were used to further validate the utility of MIP platform. This proof-of-concept phagocytosis detection platform is useful for the rapid diagnosis of microbial infections, especially in bloodstream infections (BSIs), thus improving clinical outcomes for point-of-care management.

Introduction

One hallmark of bacterial infections is the phagocytic uptake of pathogens by immune cells for targeted destruction. However, bacteria may either adopt an intracellular lifestyle to evade immune detection or remain hidden in small populations of phagocytes. Due to the technical difficulties in separating rare bacteria-internalized phagocytes from other white blood cells (WBCs), this results in poor detection of early infections. In immunocompromised individuals, such as the elderly, children, and patients with acquired immunodeficiency syndrome or cancer, sudden escalation in disease severity often lead to rapid deterioration, severe complications, and even death if gone undetected [1]. Lengthy routine diagnosis involving blood culture, PCR, fluorescence *in situ* hybridization for imaging or flow cytometry over hours to days, often delays and reduces diagnosis efficiency [2].

Phagocytes often undergo complex cytoskeleton remodeling, membrane trafficking, and cytokine signaling during the formation of pseudopodia and engulfment of pathogens [3]. While mechanical forces of phagocytes' pseudopods during formation and particle uptake were previously measured [4, 5], the overall mechanical effect on phagocytes containing internalized bacteria remains unclear. This also raises a significant question if we can harness such mechanical changes after phagocytosis to isolate and concentrate small numbers of bacteria-internalized phagocytes from large populations of host cells, with the ultimate aim of detecting early or intracellular infections rapidly in a label-free manner.

Here, we first demonstrated that human monocytes, after internalizing various bacterial pathogen species, had an overall increase in mass and cell stiffness, using microscopy measurements and a microfluidic-based deformability assay, respectively. There is no prior study conducted to demonstrate a correlation of phagocytic cell stiffness with bacterial phagocytosis to the best of our knowledge.

Leveraging the mechanical differences in bacteria-internalized monocytes and uninfected monocytes, we developed a microfluidic-based biosensor based on inertial focusing to differentially detect low numbers of human monocytes with internalized pathogens (MIP) from large uninfected populations rapidly. By achieving an excellent limit of detection (LOD) of 1 bacterium to 100 human cells, this proof-of-concept phagocytosis detection platform enabled us to quantify and detect low levels of infection and intracellular infections caused by different bacterial

species including several clinical isolates from patients. We also demonstrated its potential in clinical utility by recovering low numbers of infected monocytes from spiked human blood samples within 1.5 hr. By developing the first diagnostic method that exploits the presence of bacteria-internalized phagocytes for detection of early disease or intracellular infection, we envisioned that the MIP device platform could be widely applied to other pathogens as a point-of-care (POC) strategy to detect low-grade or intracellular infections for monitoring immunocompromised individuals with potential pathogen infections.

Results

Bacteria-internalized monocytes displayed unique physical parameters from uninfected monocytes

To address the question of how the physical properties of phagocytes alter after bacterial phagocytosis, we first evaluated the range of cell sizes obtained from infected and uninfected human monocytes. We used *P. aeruginosa* as a classic example to establish an infection model for testing. *P. aeruginosa* is an opportunistic pathogen for immunocompromised individuals (such as the elderly and AIDS patients), where it frequently infects the respiratory tract, urinary tract, burns, wounds, leading to sepsis [6]. Though classically named as an extracellular pathogen, increasing evidence had also shown that *P. aeruginosa* could survive intracellularly within host cells and contribute to intracellular infections [7, 8].

We demonstrated that the size range of monocytes with internalized bacteria (MOI 10:1) was significantly larger than that of uninfected monocytes (**Figure 1A, Supplementary Figure 1**), contributing to the difference in cell focusing within the device channel. However, the size of most infected monocytes (MOI 10:1) still had some overlap with the size of uninfected monocytes, indicating that another physical parameter was also at play. Hence, we examined if infected monocytes could exhibit any variation in their deformability by employing a microfluidic-based deformability assay [9]. To simulate initial infections with low bacterial count (low infection rates) and full-blown infections with bacterial infection of most cells (high infection rates) [10, 11], samples infected at a range of MOI (from lowest of 0.1:1 to highest of 10:1) were utilized. Interestingly, we found that infected monocytes were significantly stiffer than uninfected monocytes (**Figure 1B-D**). More importantly, the stiffness of cells infected at higher MOIs (0.1:1

to 1:1) was significantly higher than that of cells infected at lower MOIs (0.01:1 to 0.1:1), indicating that the degree of infection was correlated positively to cell stiffness (**Figure 1B**).

Based on our current results, we observed the positive correlation between MOI and monocyte stiffness, with the given mathematical equations (Supplementary Figure 2). It led to more monocytes being concentrated in outlets 2-3 in the MIP platform.

We also evaluated if our findings using *P. aeruginosa* could be translatable to other bacterial species by employing *S. aureus* (representing the most common Gram-positive bacterial pathogen) and s. *S. enterica* serovar Typhimurium (representing the classical intracellular pathogen with the ability to survive intracellularly of monocytes). Expectedly, monocytes infected with *S. aureus* or s *S. enterica* serovar Typhimurium possessed different physical properties (both size and stiffness) to uninfected monocytes, which corroborated our findings in *P. aeruginosa* **(Supplementary Figure 3, Supplementary Figure 4)**. Since our observations in the change of physical properties in monocytes apply to multiple bacterial species, this raised the rationale for developing a 'universally applicable' device that can sort rare bacteria-internalized monocytes from the rest of uninfected cell populations for convenient label-free detection of infections.

Development of the MIP biosensor for phagocytosis detection

Drawing from the idea that initial focusing-based microfluidic platforms often capitalize on differences in physical properties for detection [12, 13], we developed the MIP device, which was directed to sort and enrich rare bacteria-infected monocytes from heterogeneous uninfected populations based on the differences in cell size and deformability. This enables us to detect early infection or intracellular infection at high sensitivity and low cost. The MIP device was fabricated using soft lithography methods described elsewhere [14, 15]. The device consisted of three components: (i) an inlet for sample inflow, (ii) a main curvilinear channel for cell focusing, and (iii) five outlets for the separation of cells focused at different regions across the channel cross-section (**Figure 2A**).

We demonstrated that the stiffer and larger infected monocytes were concentrated in the first three outlets, leading to a lower proportion of cells at the target outlets (Outlets 4-5) (**Figure 2B**). The differential cell separation with the MIP device was realized with the principles of inertial focusing. Briefly, monocytes in the microchip were subjected to two main forces: inertial lift force (F_L) and

Dean Drag force (F_D) [16, 17]. During device processing, cells would be focused as tightly ordered streams when F_L was balanced with F_D. Compared with smaller cells, larger cells encounter a larger F_L to balance F_D, and the cells would be driven closer to the inner channel wall. Furthermore, deformable cells would experience an additional lift force (F_{LD}) [18], pushing cells closer to the outer wall. Therefore, as particles with different sizes and deformability experienced various degrees of F_L at different lateral positions of the channel cross-section, differential focusing of the cells would occur, resulting in efficient separation at the outlets (**Figure 2C**) [18, 19].

Evaluating the operating parameters of the MIP platform

Next, we aimed to determine the parameters needed to obtain a robust cell proportion threshold in the target outlets, using samples of uninfected monocytes with the MIP platform.

First, we processed various cell concentrations ranging from 0.01×10^6 cells ml^{-1} to 2×10^6 cells ml^{-1}. We recorded the time-lapse frames of their focused streams in the device to investigate the optimal concentration of monocytes. Before being processed through the channel, the cells were pre-stained with Calcein-AM dyes (**Figure 3A, Supplementary Figure 5A**). In the absence of bacterial infection, there was no significant difference in cell diameter for uninfected monocytes (15.51 ± 3.25 μm). In this way, uninfected monocytes were more evenly distributed across the outlets, albeit more cells were concentrated in Outlets 2-3 due to a higher flow rate within these channels (**Supplementary Figure 5B**). We demonstrated that as the cell concentration increased, the focused cell bandwidth across the channel cross-section would widen (**Figure 3B**). Specifically, samples with a cell concentration higher than 1×10^6 cells ml^{-1} would result in diffused cell bandwidths of > 80 μm, which was wider than the minimum feature size of the MIP device platform, thereby affecting the separation efficiency at the outlets. Therefore, the optimal cell concentration for these samples will be under 1×10^6 cells ml^{-1}.

We determined the proportion of uninfected monocytes in the target outlets (Outlets 4-5) of samples with various cell concentrations under 1×10^6 cells ml^{-1} (0.033×10^6 cells ml^{-1} to 0.166×10^6 cells ml^{-1}). We demonstrated that for samples with a cell concentration range of 0.1×10^6 cells ml^{-1} to 0.166×10^6 cells ml^{-1}, the proportion of cells in the target outlets was consistently higher (8.17 - 8.71 %). The proportion of cells in the target outlets was negligible for samples with a cell concentration below 0.1×10^6 cells ml^{-1} (2.0 - 2.86%) (**Figure 3C**). Therefore, the optimal range

of cell concentration for processing using the MIP device platform was 0.1×10^6 cells ml^{-1} to 1×10^6 cells ml^{-1}. Due to the advantages of microfluidics, a small sample volume was required, and the optimal cell concentration of 0.1×10^6 cells ml^{-1} was equivalent to 1 ml of blood. Due to the observed overlapping range of cell proportion in target outlets, a cut-off value of 25 percentile was used to distinguish samples with infected monocytes clearly. Therefore, we determined the threshold of the proportion of cells in the target outlets of uninfected samples as 7.10%.

The Reynolds number is affected by the flow rate, which influences the particle sorting efficiency [20]. We demonstrated that as the flow rate increased, the focused bandwidth and equilibrium position of the cells were affected (**Figure 3D**). Specifically, at lower flow rates (< 1.7 ml min^{-1}), the focused bandwidth across the channel cross-section would be more diffused (1.3 ml min^{-1}: 101.53 ± 2.39 μm, 1.5 ml min^{-1}: 57.52 ± 1.31 μm) (**Figure 3D**). The cell bandwidth obtained at a flow rate of 1.7 ml min^{-1} was consistently focused within the range of 25.5 ± 0.90 μm. At flow rates > 1.7 ml min^{-1}, the equilibrium position of the focused bandwidth would also fluctuate and shift closer to the inner wall of the device channel. Therefore, we used a flow rate of 1.7 ml min^{-1} in our subsequent experiments to ensure cell focusing and separation consistency.

Due to the brief passage of cells through the MIP device platform, we hypothesized that the shear stress experienced by the cells during the enrichment process was negligible. To evaluate this, we analyzed the viability and morphology of the cells before and after enrichment using Calcein-AM dyes. We demonstrated no significant difference in the viability of monocytes before and after sorting (> 93% viability; **Figure 4A**). The cell morphology was also largely conserved with no visible physical changes or aberrations to cell viability (**Figure 4B**), which indicated that the shear stress on the cells during processing was negligible.

Next, we showed that single bacteria would not be subjected to differential forces in the channel because the differences in size and deformability were negligible. We employed a *P. aeruginosa* strain engineered to constitutively produce the green fluorescent protein (GFP) for convenient observation and confirmation of our findings [21]. GFP expression was used to verify the presence of infection and validate the multiplicity of infection (MOI; bacterium: monocyte) (**Figure 4C**). We found that fluorescence readings above 1.01 reflected the presence of monocytes infected with *gfp*-tagged bacteria. Using the fluorescence intensity threshold value of uninfected monocytes (1.01; **Supplementary Figure 6A**), we determined that the average fluorescence intensity of a

single *P.aeruginosa* bacterium was 1.56 ± 0.07 arbitrary unit (A.U). As shown by the quantification of colony-forming units (CFU), we found that the extracellular bacteria were evenly distributed across the device outlets (**Supplementary Figure 6B**). Therefore, the MOI of a sample could also be estimated based on the difference between the CFU counts obtained from Outlets 2-3 and the averaged CFU count obtained from samples of Outlets 1-5.

Label-free detection of low-level infections based on the presence of infected monocytes

After sorting the bacteria-internalized monocytes, we aim to validate the MIP platform for detecting low-level infections without the need for biomarker labeling. We first quantified the bacteria-internalized monocytes sorted to each outlet of the MIP device platform to determine the recovery rate and sorting efficiency of these monocytes from the uninfected populations. The actual MOI was determined by dividing the total fluorescence intensity of monocytes by the average fluorescence intensity of an individual bacterium (1.56 A.U., **Supplementary Figure 6A**) monocyte count. For the convenience of labeling infection severity, samples of varying MOIs were classified into two degrees of infection, higher (0.1:1 to 1:1) and lower (0.01:1 to 0.1:1) infection rates (**Supplementary Figure 1A-D**) [22].

We demonstrated that samples with a higher proportion of infected monocytes due to higher infection rate (MOI 0.1:1 to 1:1) led to a lower average proportion of cells in the target outlets (Outlets 4 and 5) than the lower infection rate samples (reduction by 3.52 times) (**Figure 5A, Supplementary Figure 7A-B)**. Compared with the uninfected controls, samples at a lower infection rate (MOI 0.01:1 to 0.1:1) also had a lower average proportion of cells at the target outlets (reduction by 1.46 times). For samples infected at MOI > 0.1:1, the threshold of the proportion of cells in target outlets was 4.50%. The stiffer cells were more concentrated in Outlets 2 and 3 (**Supplementary Figure 7C-D**), as shown by CFU count. The distinct thresholds demonstrated with higher and lower infection rate samples showed that the MIP device platform could identify positively infected samples and distinguish samples infected at various degrees of infection.

The MIP platform can detect infections from different bacterial species

To demonstrate the applicability of the MIP device for various bacterial infections, we also evaluated the proportion of cells in target outlets with samples infected by *S. aureus* or s. *S. enterica* serovar Typhimurium. As demonstrated similarly with single *P. aeruginosa* cells (**Supplementary Figure 6B***)*, even distribution of single *S. aureus* and s. Typhimurium cells was also observed **(Supplementary Figure 8).** For bacteria-infected samples, infected monocytes were similarly concentrated within Outlets 2-3 due to the higher flow rate within these channels (**Supplementary Figure 9**). The average fluorescence intensity of a single *S. aureus* bacterium was 1.25 ± 0.1 A.U (**Supplementary Figure 6A**). As with samples infected with *P.aeruginosa,* the stiffer cells infected with s. Typhimurium were more concentrated in Outlets 2 and 3, as shown by the CFU count (**Supplementary Figure 10**). We determined that the thresholds of cell proportion within the target outlets for *S. aureus* and s. Typhimurium samples infected at lower MOI (> 0.1:1) were 5.85% and 3.70%, respectively **(Figure 5B-C)**. Similar to *P.aeruginosa*, distinct thresholds of cells within target outlets infected at higher MOI (> 1:1) could be obtained with samples infected by *S. aureus (*2.00%) and s. Typhimurium (1.08%). Interesting, we were able to distinguish samples infected with s. Typhimurium with even lower infection rates than those infected with *P.aeruginosa* or *S. aureus* (4.58 ± 0.45%, MOI 0.01:1), probably due to the intracellular nature of s. Typhimurium (**Supplementary Figure 11**). The device was validated with clinical isolates from cystic fibrosis patients with *P. aeruginosa*-based pneumonia (n = 2) [23], which reflected a consistent efficiency rate and utility of the device for clinical applications.

We further hypothesized that internalized viable bacteria were required for a positive readout with the MIP device (**Figure 5D-F**). To validate this, we quantified the proportion of cells obtained from a series of controls, using samples infected with *P. aeruginosa, S. aureus,* and s. Typhimurium. We first demonstrated that dead cells did not affect the overall distribution of cells at the outlets and that the proportion of dead cells in each outlet was evenly distributed (**Supplementary Figure 12**). We further demonstrated that in the absence of internalized viable bacteria, monocytes incubated with untreated LB media (8.59 ± 1.24%) were comparable to that of uninfected samples (**Supplementary Figure 13**). Besides, samples activated by conditioned media from bacterial cultures (*P. aeruginosa:* 7.51 ± 2.53%; *S. aureus:* 10.40 ± 0.62%; s. Typhimurium*:* 7.48 ± 0.18 %) or treated with heat-deactivated bacteria (*P. aeruginosa:* 8.04 ± 1.11%; *S. aureus:* 7.98 ± 1.37%; s. Typhimurium*:* 6.36 ± 0.87%) did not lead to significant differences in cell proportion within target outlets compared to that of uninfected samples **(Figure**

5D-F, Supplementary Figure 14). In these control samples, the proportion of cells within target outlets was also significantly higher than the 4.5% threshold previously established for samples infected at MOI > 0.1: 1. These observations confirmed that only the internalization of viable bacteria by monocytes would generate a positive outcome.

To provide further validation of the MIP platform for detecting bacterial infections from blood samples, two other bacterial species common to cause bloodstream infections, *Streptococcus agalactiae* and *Klebsiella* pneumoniae were also used[24]. We first demonstrated the even distribution of single *S. agalactiae* and *K. pneumoniae* cells in each outlet **(Supplementary Figure 15)**. Then the trend that infected stiffer monocytes will focus on outlet 2-3 was also confirmed in samples infected with both *S. agalactiae* and *K. pneumoniae*, as indicated by the CFU count (**Supplementary Figure 16, 17**). We further determined the distinct thresholds of monocytes within target outlets for samples infected with *S. agalactiae* and *K. pneumoniae* at lower MOI (> 0.1:1), were 4.54%, and 5.05%, respectively **(Figure 5G-H)**. Specifically, the thresholds of monocytes count within target outlets infected by *S. agalactiae* (3.04%) and *K. pneumoniae* (1.85%) at higher MOI (> 1:1) were also obtained **(Figure 5G-H)**.

Validation of the MIP platform with spiked human blood samples

We also demonstrated the clinical potential of the MIP device in another aspect. Using small volumes of whole human blood is also ideal for the convenient diagnosis of infections. Whole blood constitutes a wide range of cells, including red blood cells (RBCs), platelets, neutrophils (70-80%) [25] and leukocytes [26], with the monocytes accounting for 4.5-11 $\times 10^6$ cells ml^{-1} in the blood [26]. Therefore, the threshold of cell proportion obtained in the target outlets could vary from patient to patient.

We first used whole blood samples to process briefly with an RBC lysis procedure described previously, and the MIP device processed the resulting nucleated cell fraction (**Figure 6A**). We first demonstrated that in the absence of infected monocytes, the proportion of cells in target outlets (Outlets 4-5) for healthy blood controls was already higher than that previously established with monocyte samples (34.96 ± 1.70%, **Supplementary Figure 18**). This was due to the diameter heterogeneity of other WBC types in blood. We then seek to test blood samples spiked with clinically relevant proportions of bacteria-internalized monocytes (**Supplementary Figure 19**).

Next, we prepared cell concentrations corresponding to infected monocytes fractions in blood, adjusted to fit our predetermined optimal cell concentration range (0.1-1 × 10^6 cells per ml, **Figure 3B-C, Figure 6B**). Similarly, in the presence of infected monocytes, the proportion of cells in target outlets for blood sample controls was higher than that of the monocyte samples (25.21 ± 2.95%, **Supplementary Figure 20**). These observations confirmed the need to determine a personalized threshold for each clinical sample.

We hypothesized that the personalized threshold could be obtained by determining the threshold baseline that could be obtained for each clinical sample. We used blood??? samples infected with bacteria at varying MOIs and assessed the proportion of cells in the target outlets to demonstrate this method. Monocytes infected at MOI = 10:1 (0.1 X dilution), MOI = 1:1 (1X dilution) and MOI = 0.1:1 (10X dilution) and MOI = 0.01:1 (100 X dilution) were spiked into blood samples. Due to the presence of blood cells, the actual degree of infection simulated with these samples would be much lower than the MOI used.

We demonstrated that the serially diluted samples spiked with monocytes infected at MOI = 10:1, MOI = 1:1, MOI = 0.1:1, and MOI = 0.01:1 resulted in cell proportion within target outlets of 18.66 ± 1.61%, 23.16 ± 1.48%, 27.97 ± 3.88% and 27.65 ± 1.77%, respectively (**Figure 6C**). For the last two samples (MOI = 0.1:1 and MOI = 0.01:1), the difference between the proportion of cells in the target outlet was negligible, indicating a baseline value of 27.81% be obtained from the average threshold. The baseline value would reflect the proportion of cells in the blood sample without the presence of infected monocytes.

Using the personalized blood sample threshold, we further demonstrated that blood samples spiked with monocytes infected at a high level (MOI 10:1) and low-level infections (MOI 1:1) led to distinct thresholds of 21.00% and 27.81%, respectively (**Figure 6D, Supplementary Figure 21**). The distinct thresholds obtained from blood samples demonstrated that the MIP platform could isolate and concentrate rare bacteria-internalized monocytes in blood samples.

To determine if other white blood cells (WBCs), such as neutrophils, could internalize bacteria and affect the sorting efficacy of the MIP platform. We isolated WBCs from blood after RBC lysis for subsequent bacterial infection. Similar to the spiked monocyte infection test, *gfp*-tagged *P. aeruginosa* was used to infect the WBCs for 2 h and the actual MOI was determined based on the average fluorescence intensity of an individual bacterium (1.56 A.U., **Supplementary Figure 6A**).

Similarly, we also demonstrated that more WBCs would concentrate in outlets 2-3 when infected at a higher MOI (0.1:1 to 1:1) rate compared to a lower MOI (0.01:1 to 0.1:1) rate (**Supplementary Figure 22**). As described previously, the threshold to distinguish infected and uninfected sample was set as 34.96% (**Figure 6C, Supplementary Figure 18**). For samples infected at MOI > 0.1:1, the threshold of the proportion of cells in target outlets was 19.22% (**Figure 6E)**.

Clinical validation of the MIP platform with patient-derived isolates

It is important to evaluate the potential of the MIP device for clinical utility. Similar with the laboratory cultured strains, *P. aeruginosa* clinical isolates CF173-2005 and CF273-2002 [23]were used to infected monocytes and the proportion of cells in target outlets after infection were evaluated. For clinical isolates, we first confirmed that the evenly distribution trend in each outlet for both single *P. aeruginosa* strains CF173-2005 and CF273-2002 (**Supplementary Figure 23**).

For clinical isolates-infected samples, infected stiffer monocytes were observed more concentrated within Outlets 2-3 (**Supplementary Figure 24A-B, 25A-B**), as indicated by the CFU count (**Supplementary Figure 24C-D, 25C-D**). We further determined that the thresholds of cell proportion within the target outlets for CF173-2005 infected at lower MOI (> 0.1:1) was 4.40% **(Figure 6F)**. while the distinct threshold of cells within target outlets infected at higher MOI (> 1:1) was 1.87%. Similar to CF173-2005, the thresholds of cell proportion within the target outlets for CF273-2002 infected at lower MOI (> 0.1:1) and higher MOI (> 1:1) can be obtained at 5.18% and 2.67%, respectively **(Figure 6G)**. These screens with patient-derived samples clearly reflected the clinical utility of the MIP platform, highlighting the potential of this technology in personalized management for infectious disease.

Hence, we successfully demonstrated the applicability of the MIP device to detect infected samples in a clinical setting.

Discussion

Diagnosing asymptomatic cases or infections with mild symptoms is a significant challenge caused by early-stage or intracellular bacterial infections. As bacteria can hide in host cells and evade

recognition by the immune system, false-negative readings in routine culture assays are common [27, 28]. As clinicians usually have a narrow treatment window, any treatment delay will increase disease severity and mortality [29]. This warrants the imperative need to develop a rapid, sensitive diagnosis method to detect such infections.

Here, we presented a label-free microfluidic-based phagocytosis biosensor to diagnose infections by rapidly detecting rare bacteria-internalized monocytes from non-infected host cells for detection, based on increased size and stiffness of monocytes with internalized bacteria. The MIP microfluidic platform required only simple optical imaging to generate outputs that identify infection and provide readouts within 1.5 h. Because of its ease of operations and low fabrication cost, clinicians could screen many samples in parallel under high throughput with minimal equipment requirements to identify immunocompromised individuals with potential risks of worsening infection, thereby facilitating early treatment interventions. Moreover, the optimal cell concentration required also corresponded to only a small blood sample volume (~ 1 ml), thus enabling routine screening and POC detection. We also confirmed that the MIP platform was not only applicable to monocytes, but also for the validation of neutrophils within the bloodstream.

Overall, we leveraged our novel findings in the mechanics of bacteria-internalized phagocytes to develop a robust and novel strategy to detect low-level or intracellular infections caused by different bacterial species. We envision that our proof-of-concept MIP device platform could be conveniently translated to other infections, including those caused by fungi and parasites.

Experimental Section

Bacteria and monocyte cell cultures

P. aeruginosa PAO1*, S. aureus* 15981*,* s. *S. enterica* serovar Typhimurium ATCC14028, *S. agalactiae* COH1, *K. pneumoniae* KP-1, *P. aeruginosa* clinical isolates CF173-2005 and CF273-2002 were cultured in 2 ml Luria-Bertani (LB) media (Becton, Dickinson and Company, #244620, USA) at 37 °C overnight, where bacteria concentrations would reach approximately 10^9 cells ml^{-1}. Bacteria suspensions were centrifuged at 11.8×10^3 RCF for 3 min and resuspended in 1 ml PBS. As previously reported, *gfp*-tagged *P. aeruginosa* and *gfp*-tagged *S. aureus* were used to visualize the infection of bacteria [30].

Clinical isolates used to validate the clinical utility of the platform were CF173-2005 isolate of lineage H and CF273-2002 of similar lineage, which was isolated from cystic fibrosis patients in Denmark [31].

Monocyte cell line (U937) was cultured in RPMI-1640 (Gibco, # 11875085, USA) supplemented with 10% FBS (Gibco, # 10270106, USA) and 1% penicillin-streptomycin (Gibco, # 15140122, USA). Cells were cultured in optimal conditions under a 5% CO_2 atmosphere at 37 °C under humidified conditions. Media were refreshed every 48 h, and cells were passaged at 80% confluence.

Infection assays

As previously described [32], monocytes were washed three times with phosphate buffer saline (PBS) (Gibco, # 70011044, USA) and transferred to the fresh RPMI-1640 medium + 10% PBS. Monocytes were infected with bacteria in RPMI-1640/10% FBS (no antibiotics added) at different MOI (10:1, 1:1, and 0.1:1, 0.01:1) and incubated at 37°C under 5% CO_2, 99% humidity, for 2 h. Infected samples were centrifuged at 260 RCF for 3 min and resuspended in fresh cell culture media three times to remove unbound extracellular bacteria.

Device fabrication

The fabrication of the molds was performed by photolithography, as previously described [14]. The aluminum mold was fabricated by micromachining [15]. Patterns were replicated from the mold using polydimethylsiloxane (PDMS) base (SYLGARDTM 184 Silicone Elastomer kit, Germany) by mixing the polymer with the curing agent at a ratio of 10:1. The PDMS was cured in an oven at 60 ℃ for 2 h after degassing with a vacuum pump. After curing, the PDMS layer was gently peeled off from the aluminum mold. A 5 min plasma treatment bonded PDMS layers, and the device was assembled in the oven at 80 ℃ for another 2 h. The channel width of the device was 500 μm, and the height was 200 μm at the inner and outer walls of the channel, respectively. The width of each of the five outlets was 100 μm. The length of the main straight channel is 15 mm while the length for each of the outlets is 10 mm.

For the cell deformability device, a silicon wafer was coated with protective photoresist AZ5214 (AZ Electronic Materials, Wiesbaden, Germany), followed by UV exposure. The developed silicon

wafer with photoresist was then etched by deep reactive-ion etching (DRIE). After removing the protective photoresist using acetone, the etched silicon wafer was treated with silane (Sigma-Aldrich, St. Louis, MO).

Device processing

Bonded devices were assessed for leakage before use. Samples were resuspended in 1.5 ml PBS and introduced to the MIP device platform at a flow rate of 1.7 ml min^{-1}, using a syringe pump (New Era Pump System, Inc, USA). Cells were collected from each outlet in 1.5 ml tubes.

Cell viability and immunostaining

Monocytes were stained with 5 μM Hoechst (for nuclei labeling), Calcein AM (Invitrogen, #C3100MP, USA) and 5 μM Propidium Iodide (PI) (Sigma-Aldrich, #81845, USA) respectively, and incubated under 37℃ for 30 min (Calcein AM), room temperature for 1 min (PI) to identify live and dead cells. Samples were washed with PBS before fluorescence imaging with a fluorescence microscope (Nikon, Eclipse Ci-L, Japan).

Stiffness measurement

Cell stiffness of the monocytes was quantified by our previously developed elasticity microcytometer [33]. Before the stiffness measuring experiments, the device was coated with 1% (w/w) pluronic F-127 (Sigma-Aldrich, P2443, USA) for 30 min to prevent cell adhesion. The cells were briefly injected with a steady driving pressure into confining microchannels with confining channels. The cells were trapped at a confining channel position where the channel width is narrow enough to trap the cells under the driving pressure. Micrographs of the confining channels with the trapped cells were captured under a phase-contrast inverted microscope (Nikon, Eclipse Ci-L, Japan) at 100 Pa pressure. The cell elasticity was determined by the cell size and position in the confining microchannel obtained from the micrographs. The elastic modulus of monocytes was then calculated based on the hyperelastic Tatara model, as shown in Equation (1) [9, 34]:

$$(1)\text{: E} = \frac{3(1-v^2)A}{2\left(D_{cell}-W_{deform}\right)}\left(1+\frac{2Ba^2}{D_{deform}^2}\right)\frac{F_{compress}}{a} - \frac{2A}{\pi\left(D_{cell}-W_{deform}\right)}(1 + \frac{4Ba^2}{5D_{deform}^2})\frac{F_{compress}}{f(a)}$$

Where D_{cell} is the cell diameter, D_{deform} is the deformed cell diameter, W_{deform} is the deformed cell width, v is the Poisson's ratio of a cell, a is the contact radius, and $f(a)$ is the characteristic length of the non-spherical geometry after deformation.

A and B in the above equation can be given as (2),

$$(2)\text{: A} = \frac{(1-\xi)^2}{1-\xi+\frac{\xi^2}{3}},\ \text{B} = \frac{1-\frac{\xi}{3}}{1-\xi+\frac{\xi^2}{3}},\ \xi = 1-\frac{W_{deform}}{D_{cell}}$$

Where ξ is the deformation of the cell.

Colony-forming unit (CFU) assay

As previously described [35], bacterial suspensions were collected and serially diluted for growth on an LB agar plate (Sigma-Aldrich, # L3027, USA) at 37 ℃ for 24 h to quantify bacterial counts. The CFU mL^{-1} was obtained by the average number of colonies × dilution factor × volume. The data obtained from the infection assay were normalized by dividing the average CFU value of outlets 1 and 5.

Control assays with activated monocytes

Activated monocytes were obtained by treating naïve monocytes with 0.22-μm filter-sterilized LB media conditioned with live bacteria for 2 h or exposure to heat-deactivated bacteria (MOI 10:1).

Whole blood test

Single donor human whole blood (Innovative Research, Inc, #IWB1K2E10ML, USA) was mixed with RBC lysis buffer (1:9 ratio, Invitrogen, # 00-4333-57, USA) and shaken gently for 5 min. Lysed samples were centrifuged at 500 × g for 5 min. RBC debris and plasma were discarded, and the remaining WBC pellet was resuspended into 1 ml PBS for further use.

For infection assays, infected samples at MOI = 10: 1, MOI = 1: 1 were obtained by spiking infected monocytes into blood samples after RBC lysis, followed by direct processing with the device.

For whole WBCs infection assays, WBCs were infected with *P. aeruginosa* at different MOI (0.1:1 and 1:1). The count of bacteria was determined by multiplying the experimental MOI rate and the count of whole cell numbers including the incompletely lysed red blood cells.

Imaging and analysis

Cell suspensions were collected from each outlet for imaging under a fluorescent microscope. Cells were resuspended in the 1.5 ml tube and an 18 well plate (ibidi, #81826, Germany) was used to place the mixed cell suspension. The nuclei of cells were stained by 5μM Hoechst (Invitrogen, # H1399, USA) to quantify cell recovery and cell proportions within outlets. Images of monocytes with and without internalized pathogens were obtained to characterize the cell size before and after infection, and the cell size was quantified with predetermined algorithms. All fluorescent images were processed by Image J software (National Institutes of Health, USA). Automated algorithms were used to establish cell counts and quantify intensity outputs. Fluorescent intensity was normalized to background intensity values. Data were plotted by Origin software (OriginLab Corporation, USA).

Statistical analysis

The results were expressed as means ± standard deviation. Data groups were compared using the one-way ANOVA and Student's t-test to evaluate associations between independent variables, and the P values were obtained. Three independent trials were conducted in triplicates for each experiment.

Acronyms

POC	Point-of-care
MIP	Monocytes with internalized pathogens
P. aeruginosa	*Pseudomonas aeruginosa*
S. aureus	*Staphylococcus aureus*
s. Typhimurium	*Salmonella typhimurium*
MOI	Multiplicity of infection
LOD	Limit of detection
WBCs	White blood cells
F_L	Inertial lift force
F_D	Dean Drag force
F_{LD}	Lift force induced by deformability
GFP	Green fluorescent protein
CFU	Colony-forming units
RBCs	Red blood cells
A.U	Arbitrary unit

Figures and Tables

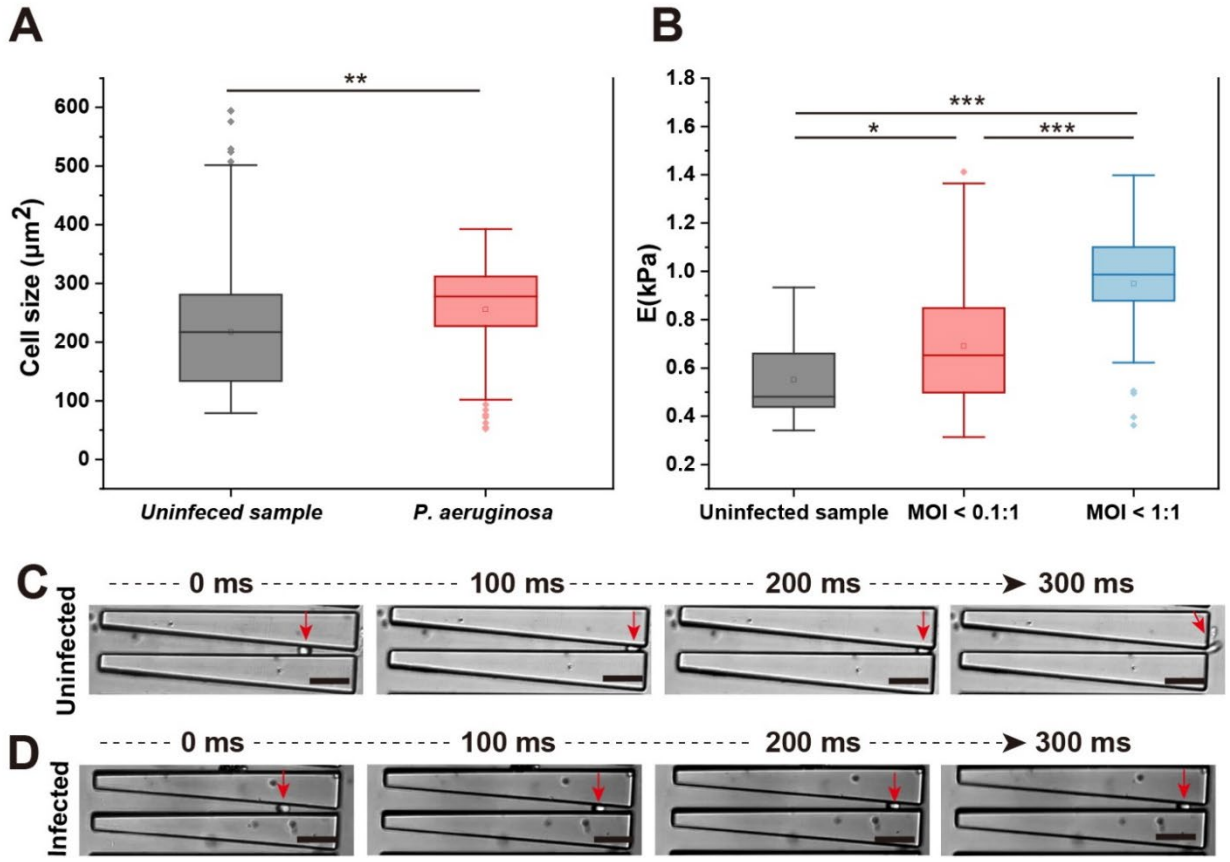

Figure 1: Stiffness of infected and uninfected monocytes. A) Size range of uninfected and bacteria-infected monocytes. B) Stiffness of uninfected and *P. aeruginosa* infected monocytes at various MOI (Uninfected: 0.55 ± 0.03 kPa; MOI < 0.1:1: 0.69 ± 0.04 kPa; MOI < 1:1: 0.95 ± 0.24 kPa), E(kPa) = Elastic modulus (kilopascals). C) Representative time lapse frames of uninfected monocytes (indicated with red arrow) passing through the device for stiffness measurements. Scale bar = 50 μm. D) Representative time lapse frames of infected monocytes (indicated with red arrow) passing through the device for stiffness measurements. Scale bar: 50 μm. * states for p values of < 0.01, ** states for p values of < 0.001, *** states for p values of < 0.0001, ms = millisecond.

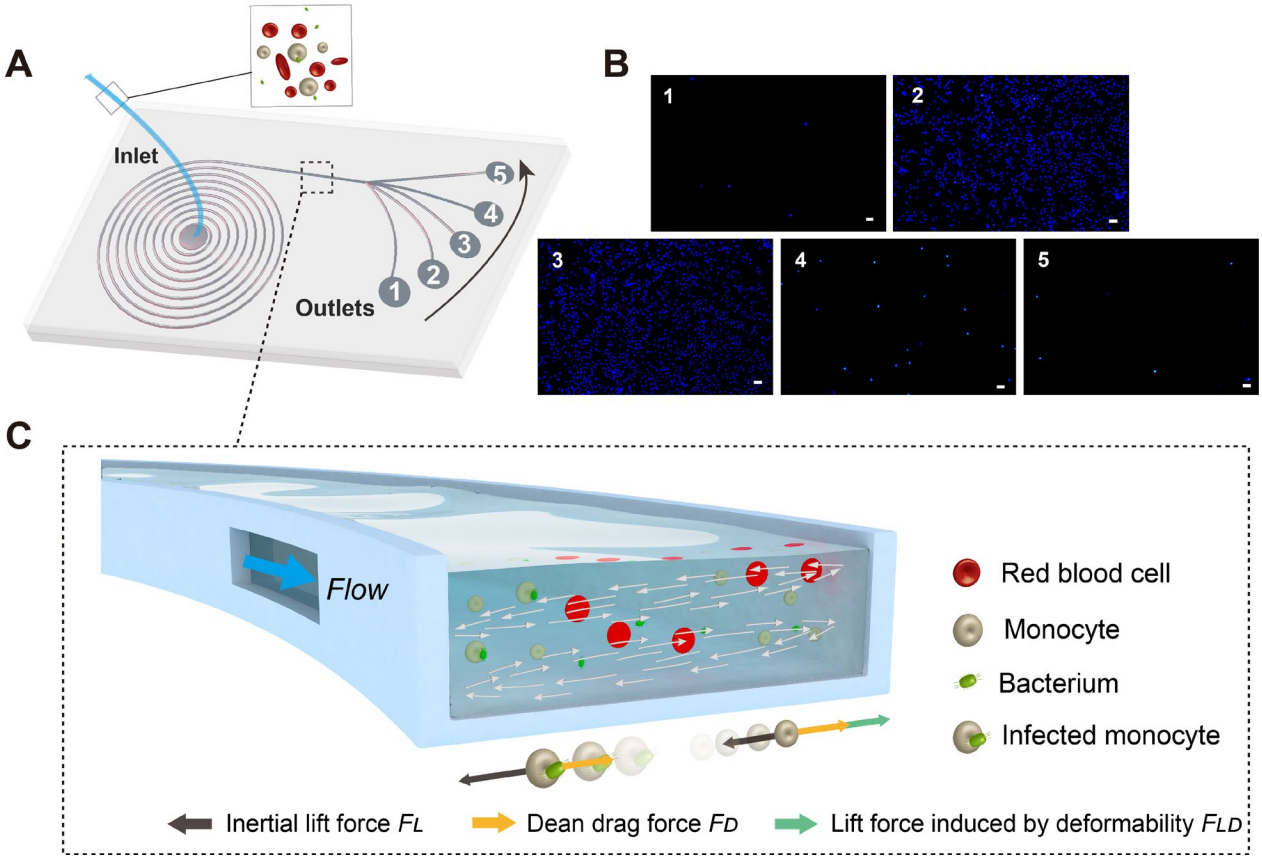

Figure 2: Label-free microchip to detect monocytes with internalized pathogens (MIP). A) Schematic diagram of the MIP device. Each microchip had one inlet and five outlets. Samples were introduced through the microchip inlet, and the sorted cells were collected from each outlet, respectively. For blood samples, nucleated cell fractions were processed after red blood cell (RBC) lysis. B) Representative images of monocytes were collected from each outlet after sorting. The proportion of cells from outlets 2 and 3 were highest due to the higher flow rate. Scale bar: 50 µm. C) Schematic diagram of force distribution within the MIP device. Deformable healthy monocytes experienced an additional lift force and moved close to the outer wall, while stiffer and larger infected cells moved close to the inner wall.

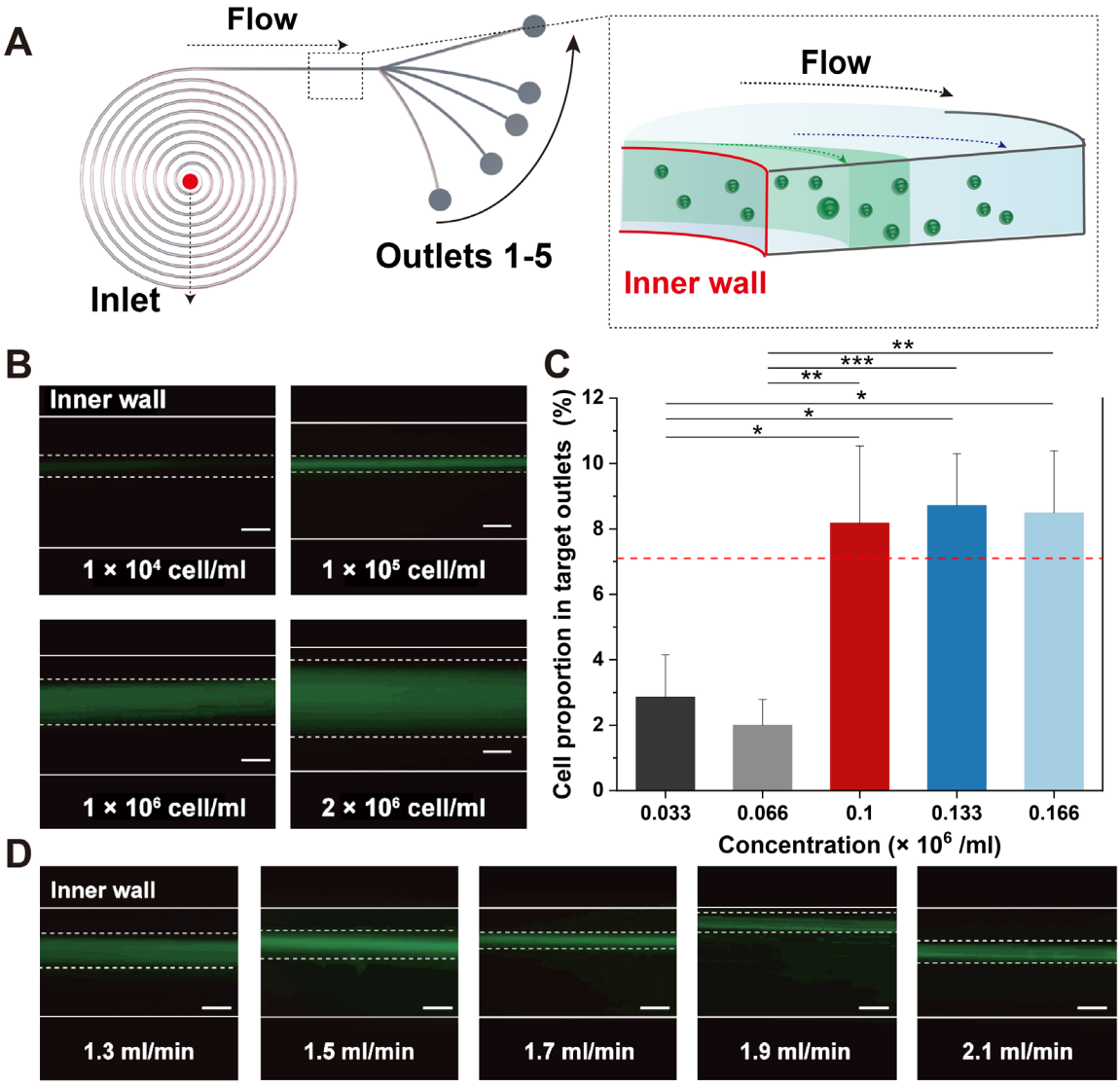

Figure 3: Evaluation of operating parameters with the MIP device platform. A) Schematic of the optimization process. B) Representative images of Calcein AM stained monocytes under different cell concentrations (1×10^4 cells ml^{-1}, 1×10^5 cells ml^{-1}, 1×10^6 cells ml^{-1}, and 2×10^6 cells ml^{-1}). White dotted lines denoted the focused bandwidths of cells. Scale bar = 100 µm. C) The proportion of cells within target outlets 4-5 for samples with different monocyte concentrations. The threshold for the proportion of cells in target outlets of uninfected samples was determined as 7.10%. D) Representative images of Calcein AM stained monocytes under different flow rates (1.3 ml min^{-1}, 1.5 ml min^{-1}, 1.7 ml min^{-1}, 1.9 m min^{-1}, and 2.1 ml min^{-1}). Scale bar: 100 µm. * states for p values of < 0.01, ** states for p values of < 0.001, *** states for p values of < 0.0001.

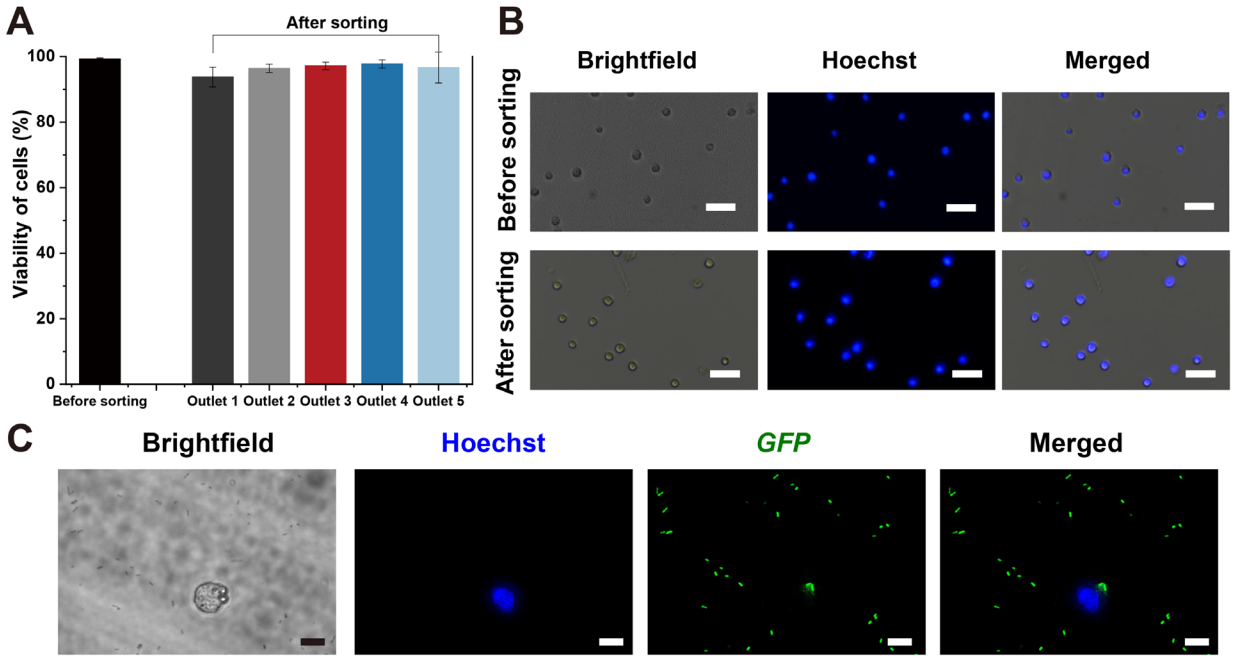

Figure 4: Characterisation of monocytes and bacteria for disease detection. A) Cell viability of monocytes before and after sorting. No significant difference in cell viability was observed. B) Morphology of cells before (above) and after (below) sorting. Scale bar: 50 µm. C) Representative images of *gfp*-tagged *P. aeruginosa* and monocytes**.** Scale bar: 10 µm.

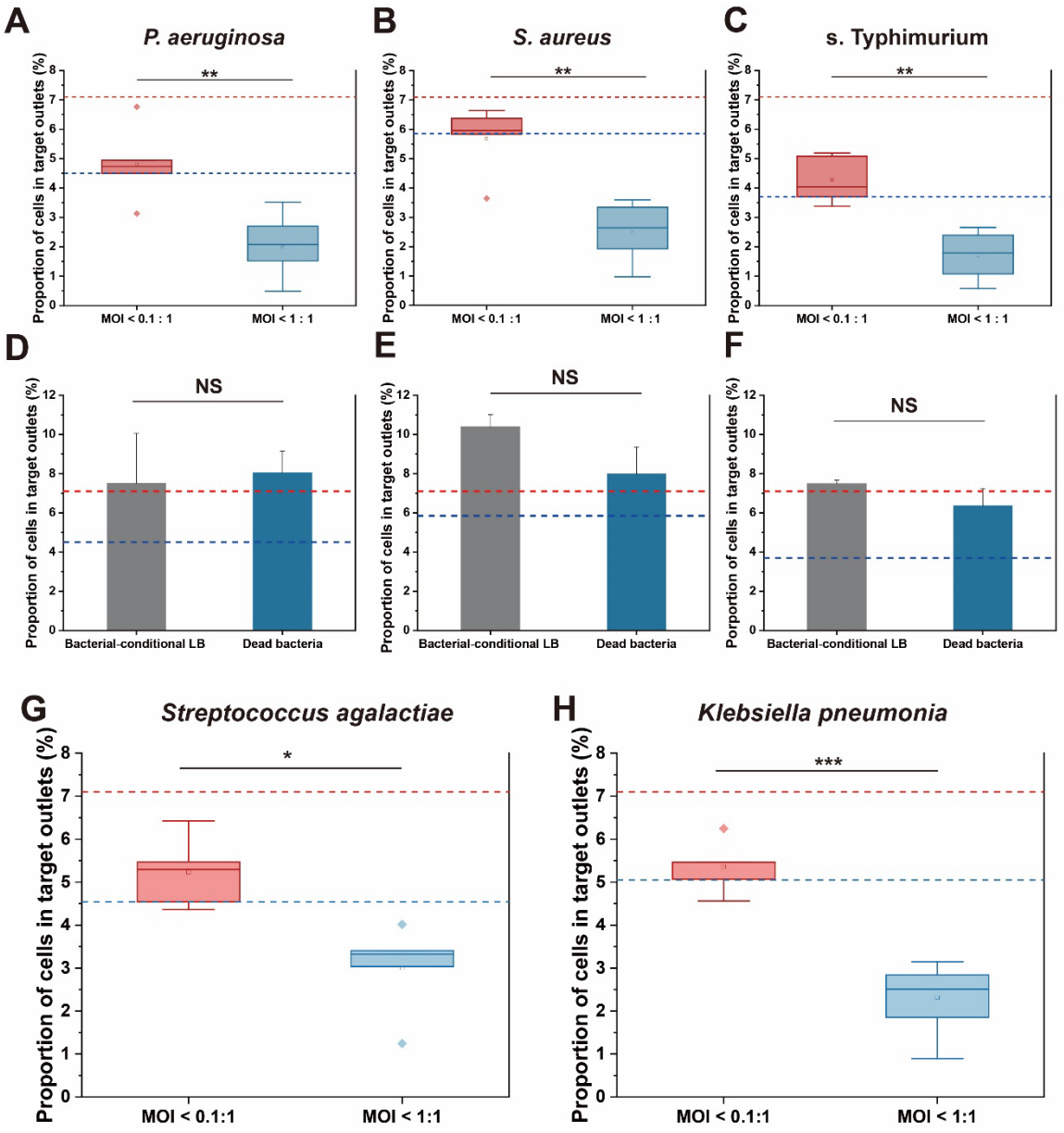

Figure 5: Detection of infection based on the proportion of cells in target outlets. The proportion of cells in target outlets for samples infected at MOI < 0.1:1 and < 1:1 with A) *P. aeruginosa* (p-value: 0.000695) and B) *S. aureus* (p-value: 0.00072) and C) s. Typhimurium (p-value = 0.001317). The thresholds of uninfected samples (7.10%) and samples infected at MOI < 0.1:1 (*P. aeruginosa:* 4.50%; *S. aureus:* 5.85%; s. Typhimurium*:* 3.70%) were denoted by the dotted red and blue lines, respectively. The proportion of cells in target outlets for samples exposed to media conditioned by bacterial cultures or exposed to dead bacteria using D) *P. aeruginosa*, E) *S. aureus,* or F) s. Typhimurium*.* The resultant proportion of cells in target outlets for each control was comparable to that obtained with healthy samples. The proportion of cells in target outlets for

samples infected at MOI < 0.1:1 and < 1:1 with G) *Streptococcus agalactiae* (p-value: 0.002526) and H) *Klebsiella pneumonia* (p-value: 0.0000053). The thresholds of uninfected samples (7.10%) and samples infected at MOI < 0.1:1 (*Streptococcus agalactiae*: 4.54%, *Klebsiella pneumonia*: 5.05%) were denoted by the dotted red and blue lines, respectively.* states for p values of < 0.01, ** states for p values of < 0.001.

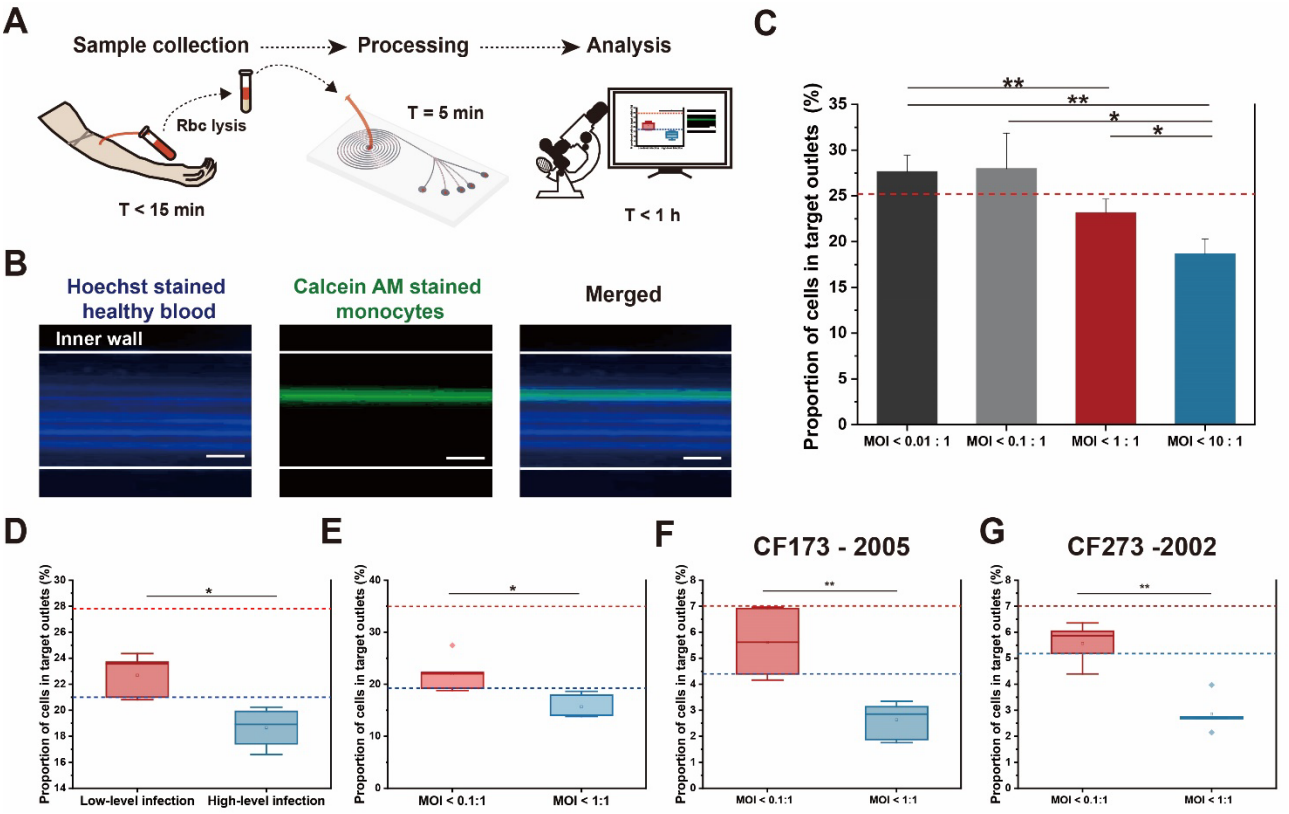

Figure 6: Validation of clinical utility with blood samples and patient-derived isolates. A) Schematic of clinical validation. B) Representative images of Calcein AM stained monocytes and Hoechst stained white blood cells in clinical samples. Scale bar: 100 µm. C) The proportion of cells for whole blood samples with spiked monocytes infected at MOI = 0.01:1, MOI = 0.1:1, MOI = 1:1 and MOI = 10:1. The dotted red line (25.21%) indicated the proportion of uninfected samples. D) The proportion of cells in target outlets for uninfected whole blood samples with spiked monocytes at low infection and high infection rates. The thresholds for samples of low infection rates (27.81%) and high infection rates (21.00%) were denoted by the dotted red and blue lines, respectively. E) The proportion of cells in target outlets for WBCs samples from whole blood infected at MOI < 0.1:1 and < 1:1 with *P. aeruginosa*. The thresholds for uninfected healthy blood samples (34.96%) and WBCs samples infected at MOI < 0.1:1 (19.22%) were denoted by the dotted

red and blue lines, respectively. The proportion of cells in target outlets for samples infected at MOI < 0.1:1 and < 1:1 with F) CF173-2005 (p-value: 0.000983) and G) CF273-2002 (p-value: 0.000371). The thresholds of uninfected samples (7.10%) and samples infected at MOI < 0.1:1 (CF173-2005: 4.40%, CF273-2002: 5.18%) were denoted by the dotted red and blue lines, respectively. * states for p values of < 0.01, ** states for p values of < 0.001.

Table 1 Comparison of MIP platform with existing technologies.

	Type	Pathogen-type	Time	Cost	Mode of detection	Ref
Culture-based	**Blood culture**	Bacteria	> 2 days	Low	Planktonic bacteria	[1, 2]
Gene-based	**Karius test (cfDNA based)**	Bacteria, virus, fungus, etc	24 h – 96 h	High	Genes	[36]
	Aptamer-Based Recognition	*S. aureus and Escherichia coli*	< 2 h	Medium	Planktonic bacteria	[37]
	Immunoaffinity mass spectrometry	*Escherichia coli, Bacillus subtilis,* and *S. aureus*	12 h	High	Planktonic bacteria	[38]
Protein-based	**Enzyme-based immunodetection assay**	SARS-CoV-2	> 24h (MOI ≥ 3:1); > 48h (MOI 1:200)	Medium	Enzymes	[39]
	Integrated Comprehensive Droplet Digital Detection system	*Escherichia coli*	1.5 – 4 h	High	Enzymes	[40]
Physical property-based	**MIP Biosensor for phagocytosis detection**	*P.aeruginosa, S. aureus,* s. Typhimurium	< 1.5 h (MOI ≥ 0.01 : 1)	Low	Intracellular bacteria	

Supplementary Information

Label-free biosensor of phagocytosis for diagnosing bacterial infections

Junchen Liao, Jifeng Ren, Raymond H. W. Lam, Song Lin Chua, Bee Luan Khoo**

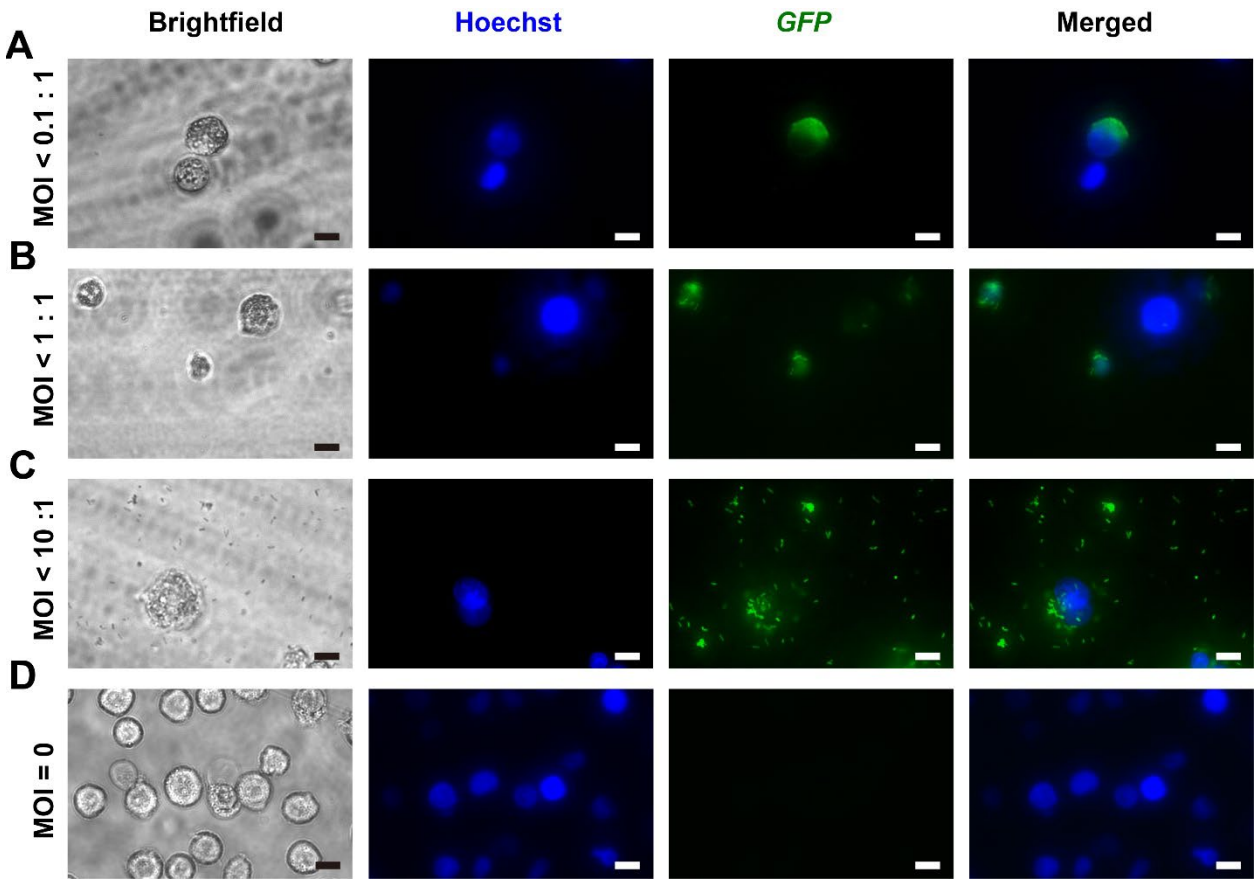

Supplementary Figure 1. Representative images of monocytes infected by *gfp*-tagged *P. aeruginosa* at A) MOI < 0.1:1, B) MOI < 1:1, C) MOI < 10:1 and D) MOI = 0. Scale bar: 10 μm.

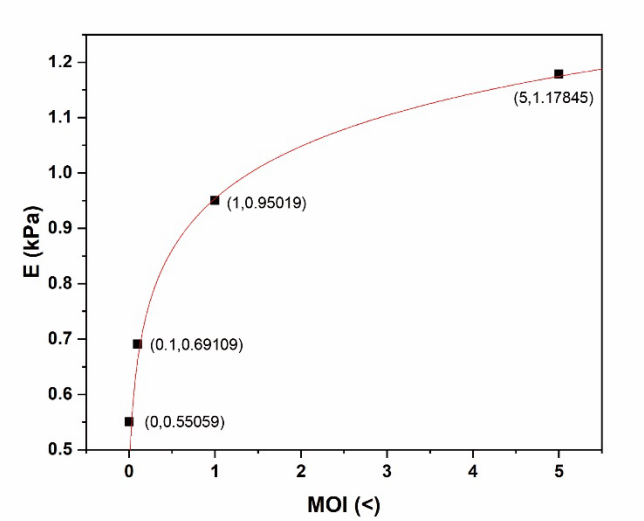

Supplementary Figure 2. The correlation between MOIs and stiffness. The data points were obtained at uninfected sample (0, 0.55059), sample infected at lower MOI (< 0.1:1) (0.1, 0.69109), middle MOI (< 1:1) (1, 0.95019) and higher MOI (< 5:1) (5, 1.17845). The given equation of MOIs and stiffness is $y = 0.95 - 0.139\ln(x + 0.02593)$.

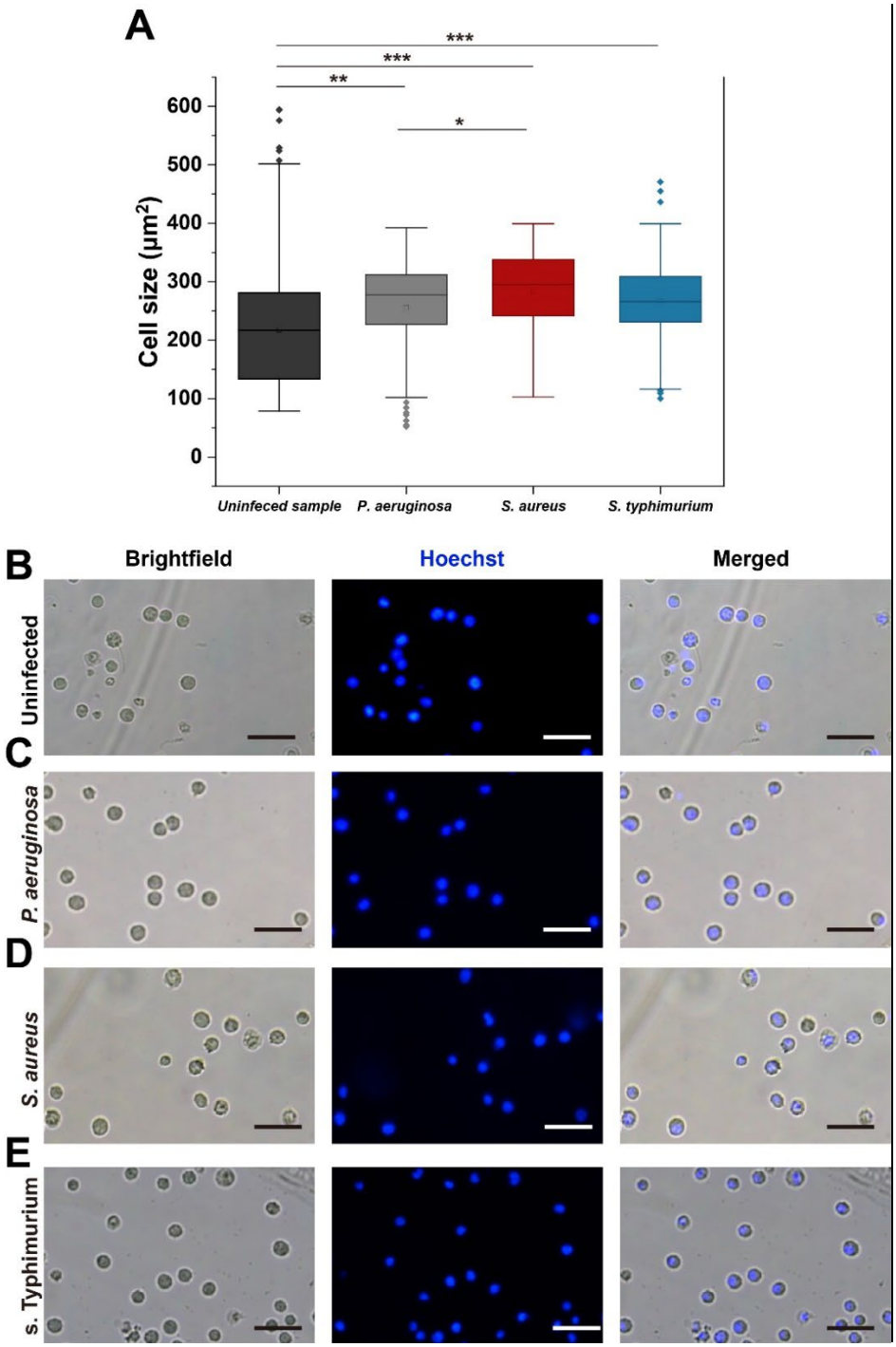

Supplementary Figure 3. Characterization of monocytes before and after infection. A) The size range of uninfected cells and cells infected by *P. aeruginosa, S. aureus,* and s. Typhimurium. Corresponding figures of B) uninfected cells and cells infected by C) *P. aeruginosa*. D) *S. aureus and* E) s. Typhimurium. Scale bar: 50 µm. * states for p values of < 0.01, ** states for p values of < 0.001, *** states for p values of < 0.0001.

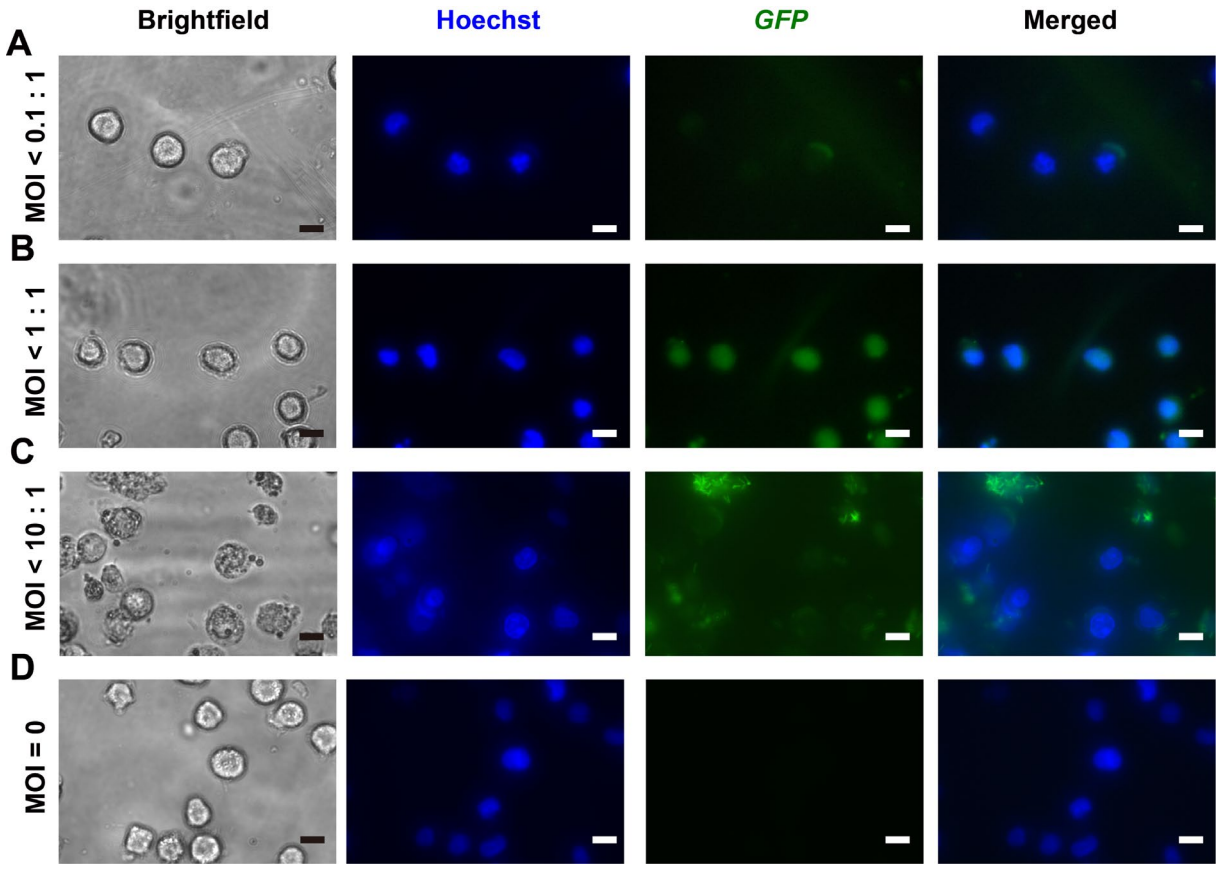

Supplementary Figure 4. Representative images of monocytes infected by *gfp*-tagged *S. aureus* at A) MOI < 0.1:1, B) MOI < 1:1, C) MOI < 10:1 and D) MOI = 0. Scale bar: 10 μm.

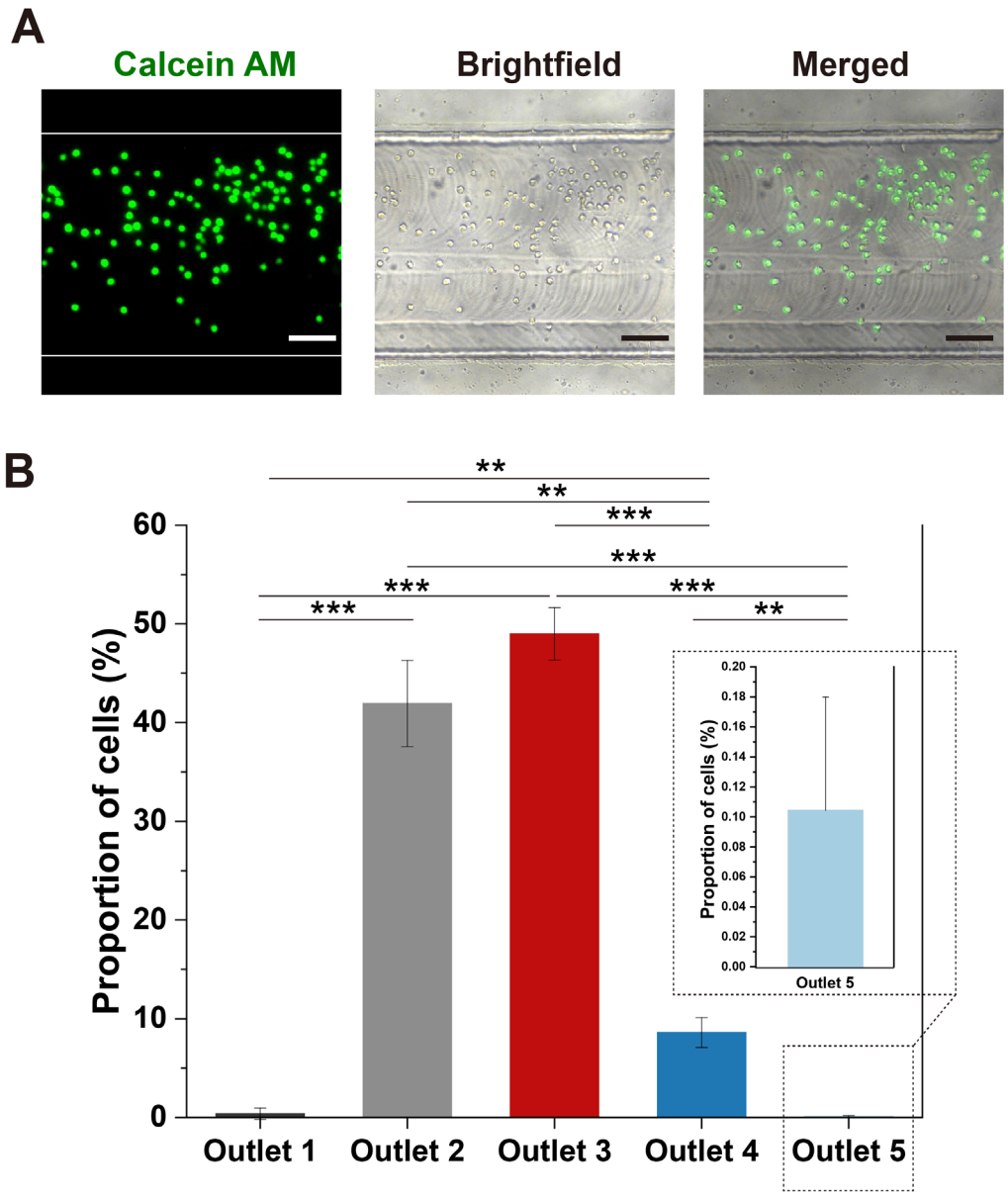

Supplementary Figure 5. Characterization of the MIP device platform. A) Monocytes in the channel of the MIP device, labeled by Calcein-AM dye. B) The proportion of cells in each outlet for uninfected samples. * states for p values of < 0.01, ** states for p values of < 0.001, *** states for p values of < 0.0001. Scale bar: 100 μm.

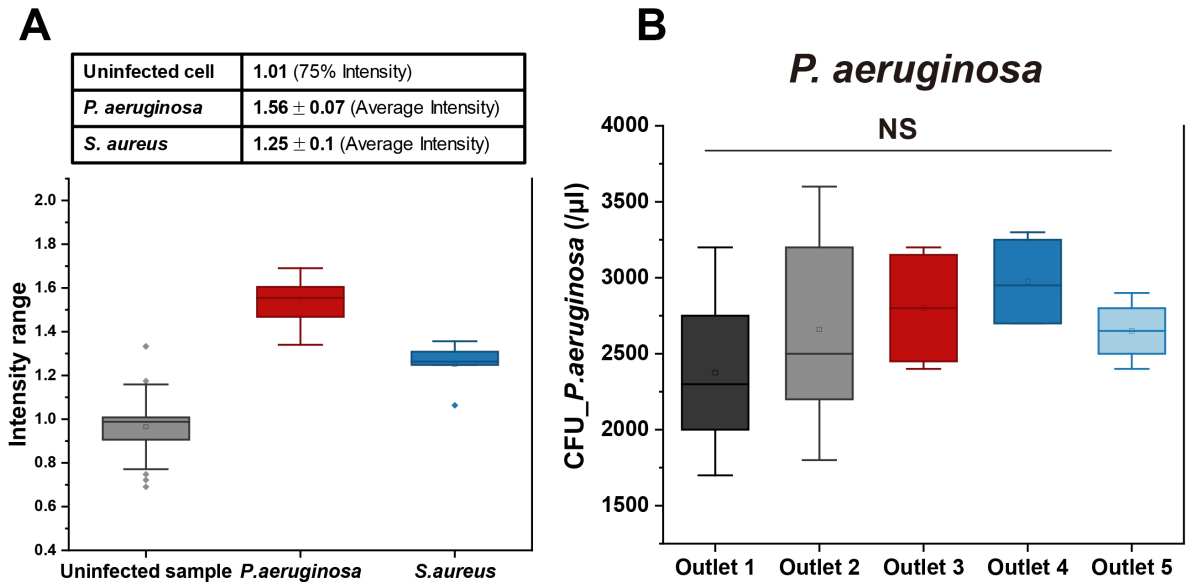

Supplementary Figure 6. Characterization of bacteria. A) The range of fluorescence intensity for uninfected monocytes and single bacteria cells. The fluorescence intensity was normalized to background intensity. The average fluorescence intensities of a single *P. aeruginosa* and *S. aureus* bacterium were 1.56 and 1.25, respectively. B) Corresponding CFU counts from each outlet for samples comprising planktonic *P.aeruginosa*. NS = not significant.

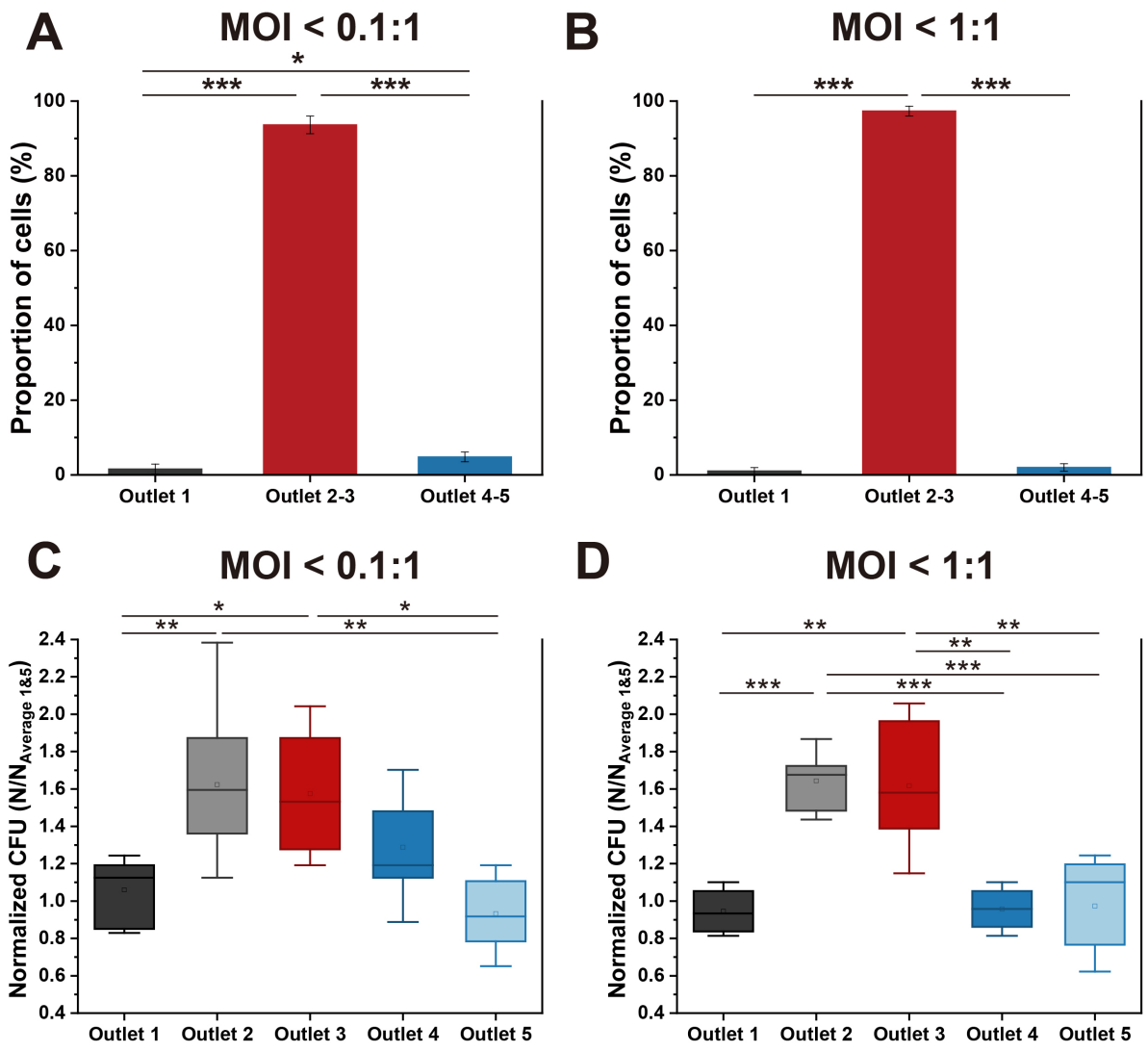

Supplementary Figure 7. Distribution of cells in the MIP device using samples infected with *P. aeruginosa*. Proportion of cells infected with *P. aeruginosa* at A) MOI < 0.1:1 and B) MOI < 1:1. Corresponding CFU for samples infected with *P. aeruginosa* at C) MOI < 0.1:1, D) MOI < 1:1. CFU data were normalized to the average CFU of outlet 1 and 5. * states for p values of < 0.01, ** states for p values of < 0.001, *** states for p values of < 0.0001.

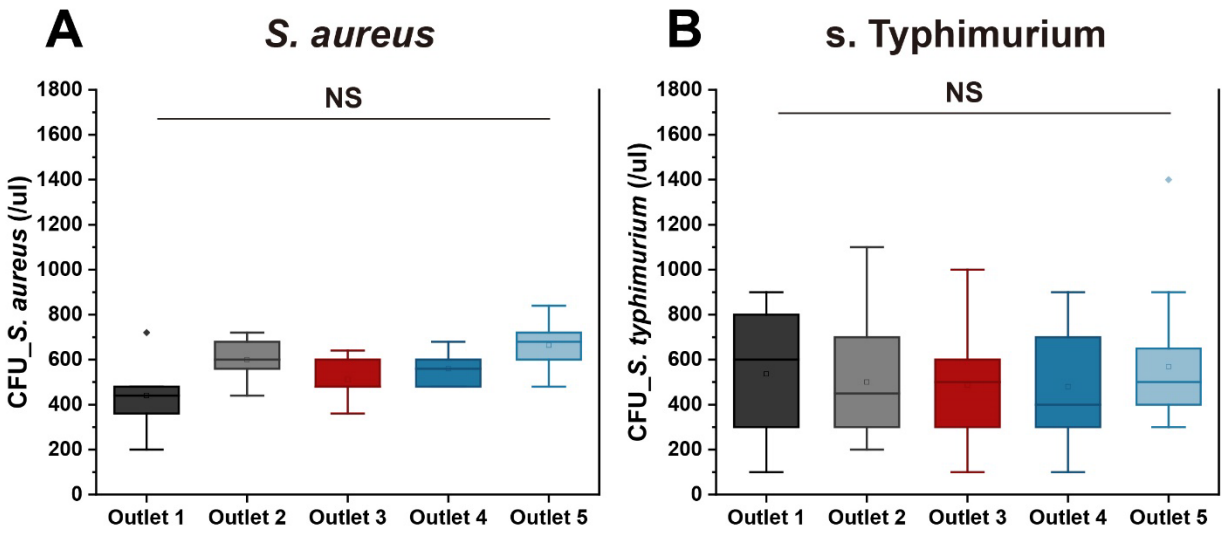

Supplementary Figure 8. Corresponding CFU counts from each outlet for samples comprising only single bacteria of A) *S. aureus and* B) s. Typhimurium. NS = not significant.

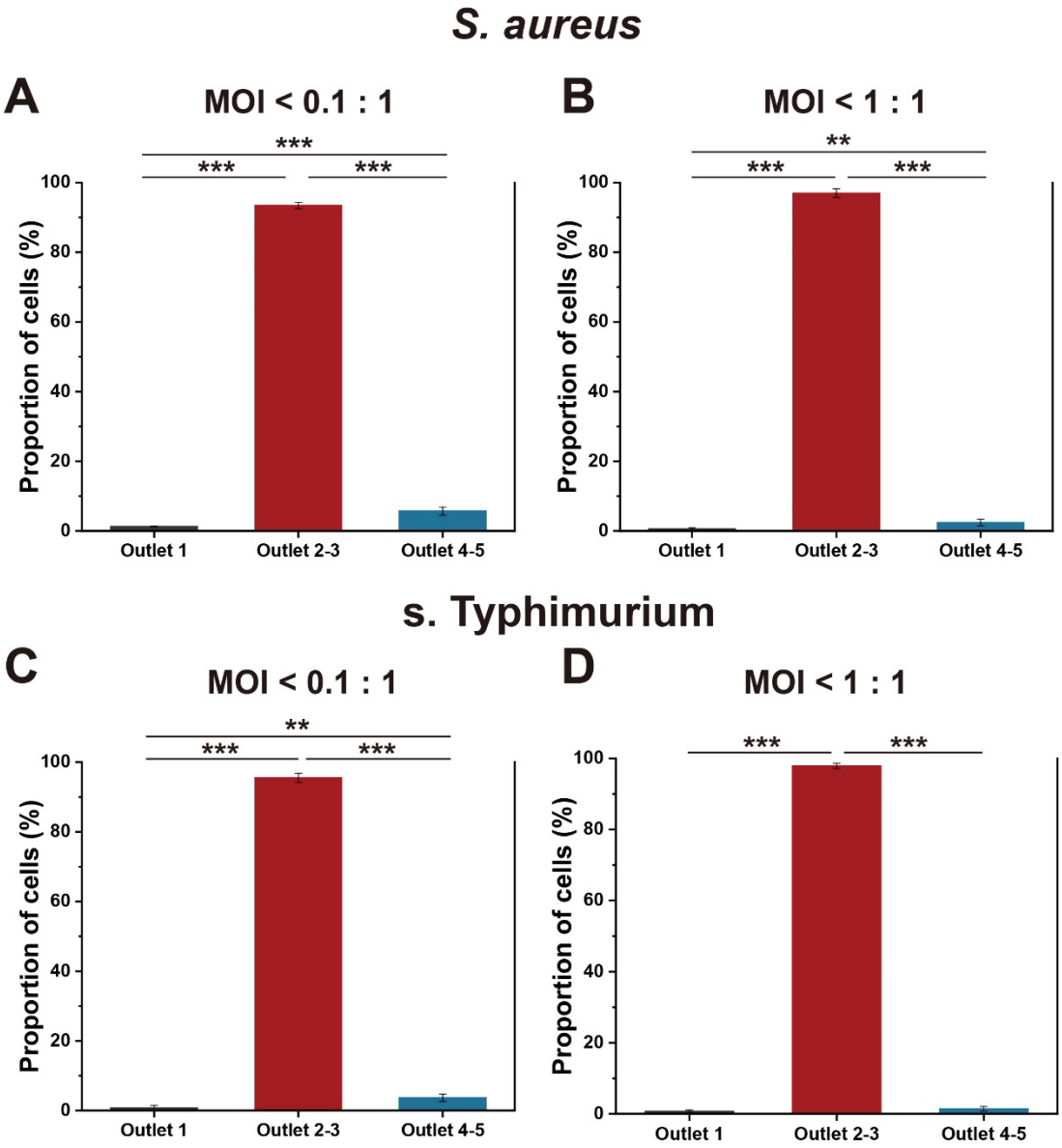

Supplementary Figure 9. Proportion of cells infected with *S. aureus* at A) MOI < 0.1:1 and B) MOI < 1:1. Proportion of cells infected with s. Typhimurium at C) MOI < 0.1:1 and D) MOI < 1:1. * states for p values of < 0.01, ** states for p values of < 0.001, *** states for p values of < 0.0001.

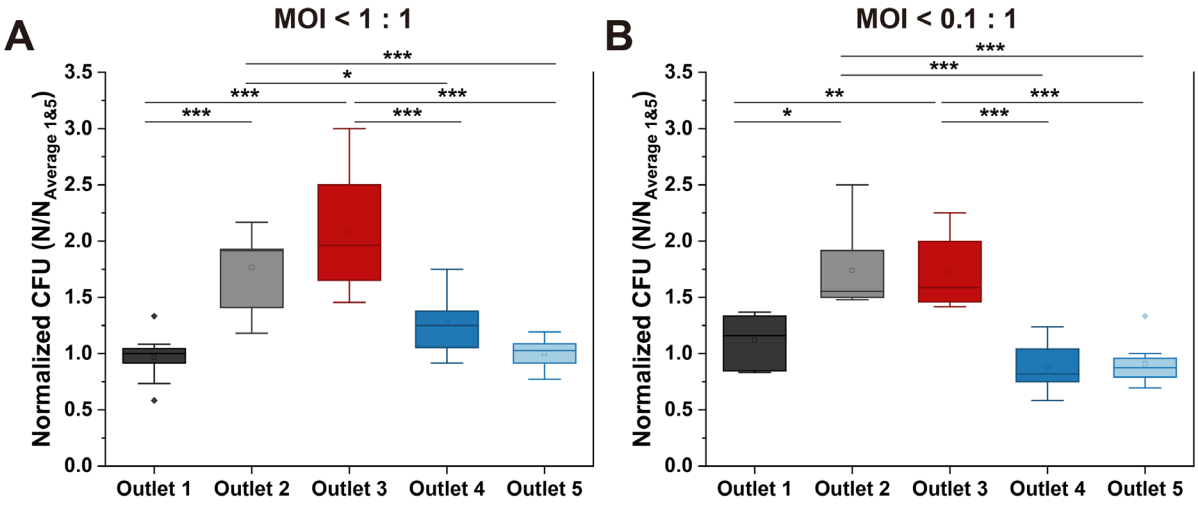

Supplementary Figure 10. Corresponding CFU for samples infected with s. Typhimurium at A) MOI < 1:1, B) MOI < 0.1:1.

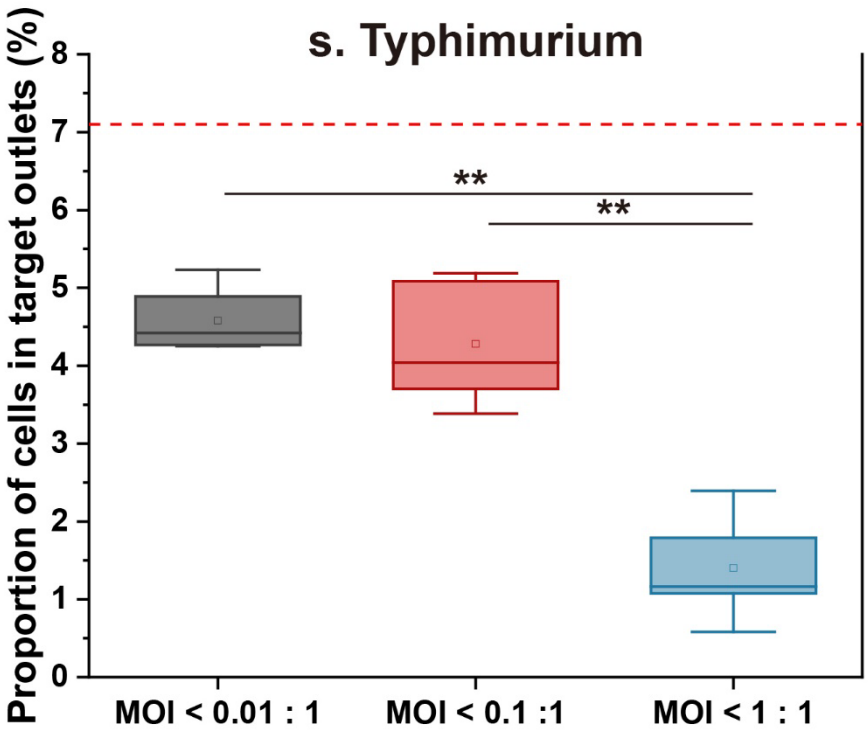

Supplementary Figure 11. The proportion of cells in target outlets for samples infected with s. Typhimurium **at MOI < 0.01:1, MOI < 0.1:1, and < 1:1.** The red dotted line indicated the thresholds of uninfected samples (7.10%). ** states for p values of < 0.001.

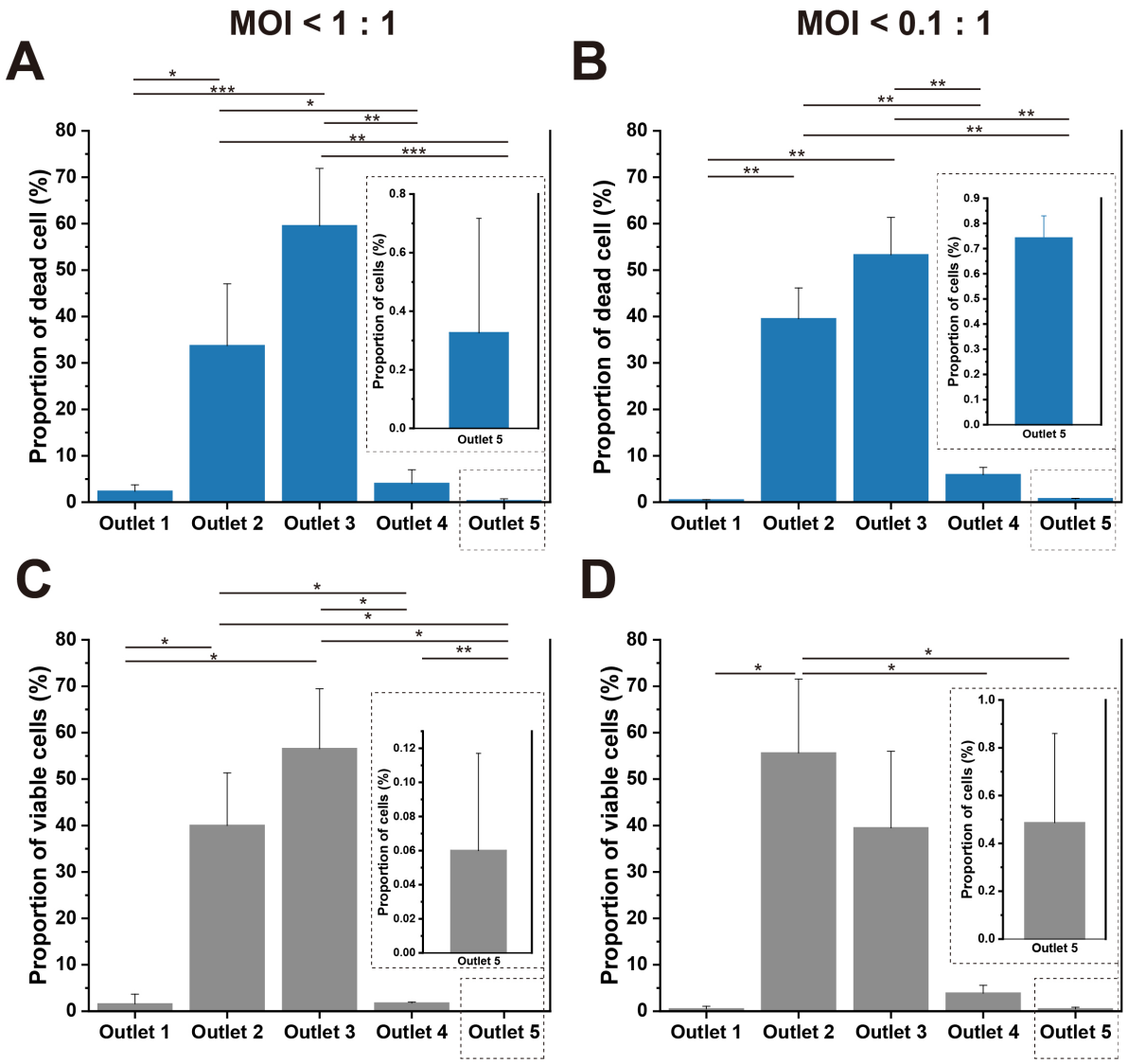

Supplementary Figure 12. Cell distribution in the MIP device platform with control samples. Proportion of dead cells across outlets for samples infected at A) MOI < 1:1 and B) MOI < 0.1:1. respectively. Proportion of viable cells across outlets for samples infected at C) MOI < 1:1 and D) MOI < 0.1:1. respectively * states for p values of < 0.01, ** states for p values of < 0.001, *** states for p values of < 0.0001.

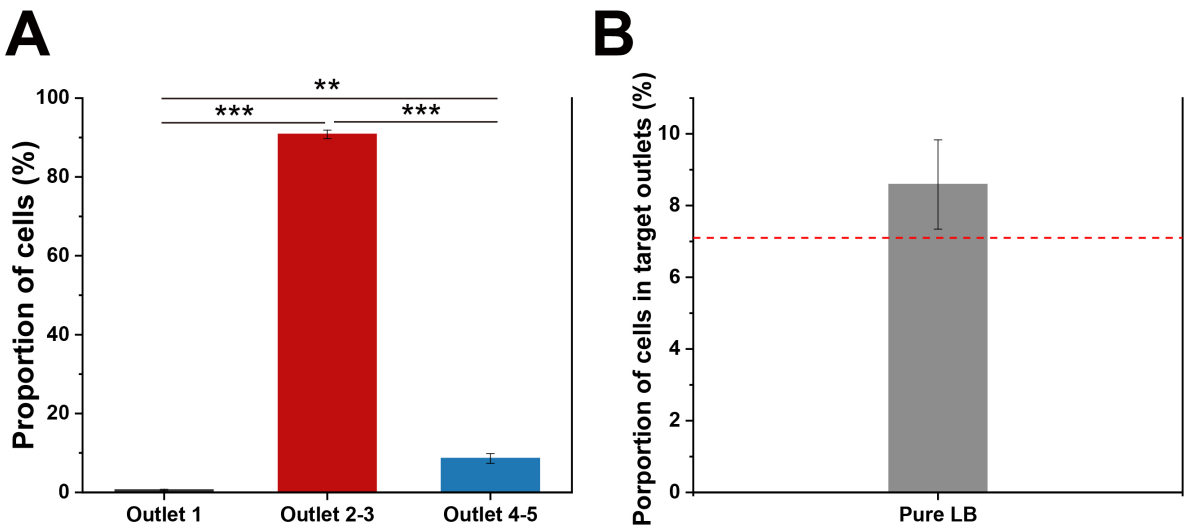

Supplementary Figure 13. Cell distribution of samples exposed to untreated LB media with the MIP device. A) Proportion of the cells in target outlets for samples maintained in untreated LB media. B) The proportion of cells in target outlets for samples maintained in untreated LB media. The result is comparable with that of uninfected samples (p-value = 0.906). Samples were processed within the optimal cell concentration as previously validated. The threshold for uninfected samples was denoted by the dotted red line, at 7.10%. ** states for p values of < 0.001, *** states for p values of < 0.0001.

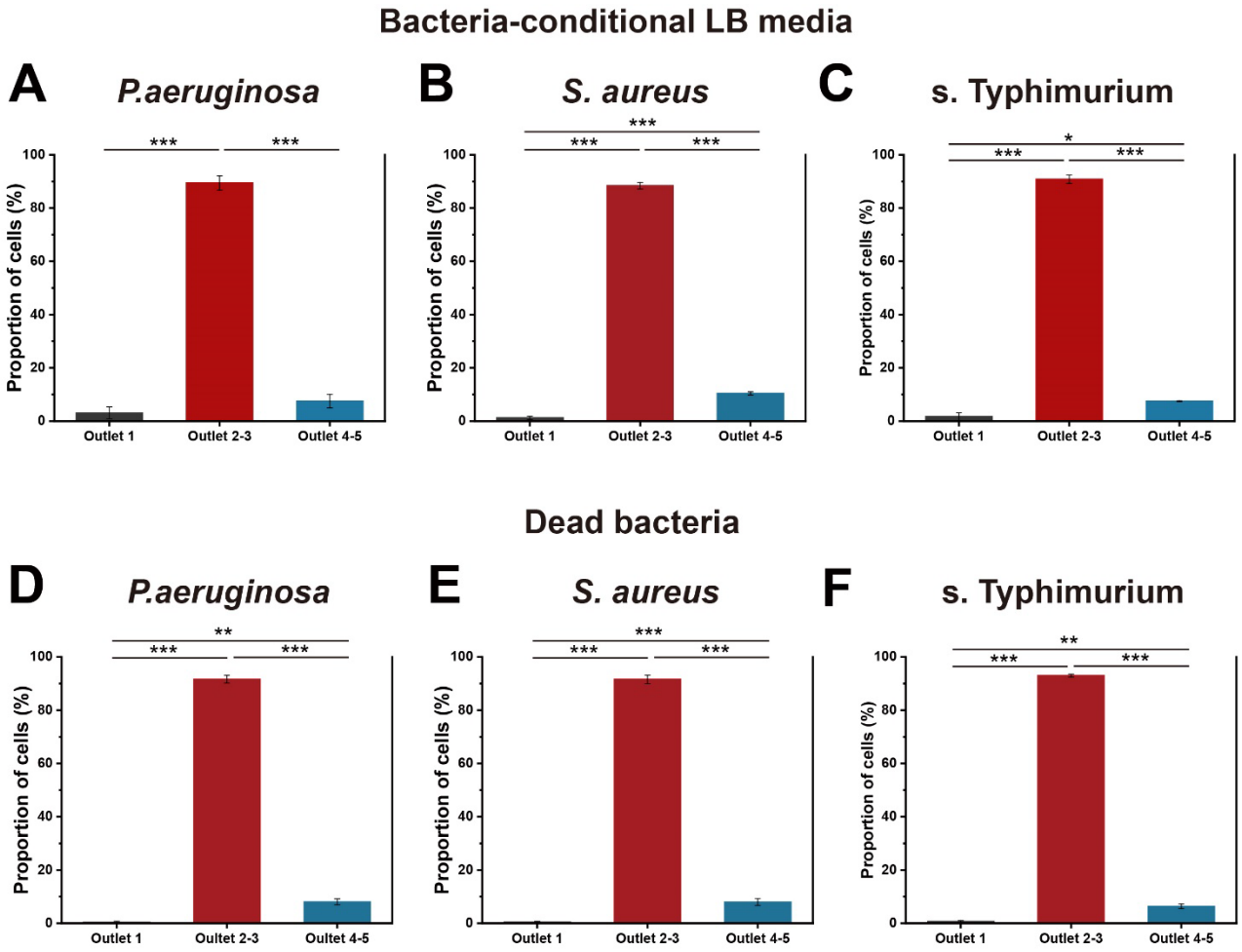

Supplementary Figure 14. Cell distribution in the MIP device using samples exposed to bacteria-conditioned LB media and dead bacteria. Proportion of cells in outlets for samples exposed to bacteria-conditioned LB media treated by A) *P. aeruginosa*. B) *S. aureus and* C) s. Typhimurium. Proportion of cells for samples exposed to samples comprising dead D) *P. aeruginosa*. E) *S. aureus and* F) s. Typhimurium bacteria. * states for p values of < 0.01, ** states for p values of < 0.001, *** states for p values of < 0.0001.

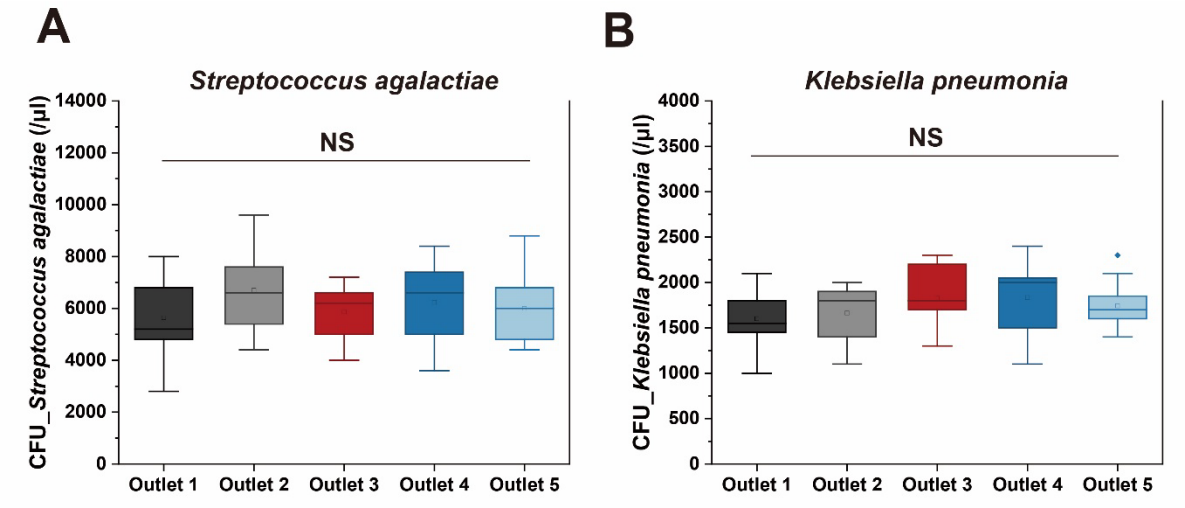

Supplementary Figure 15. Corresponding CFU counts from each outlet for samples comprising only single bacteria of A) *Streptococcus agalactiae* and B) *Klebsiella pneumonia*. NS = not significant.

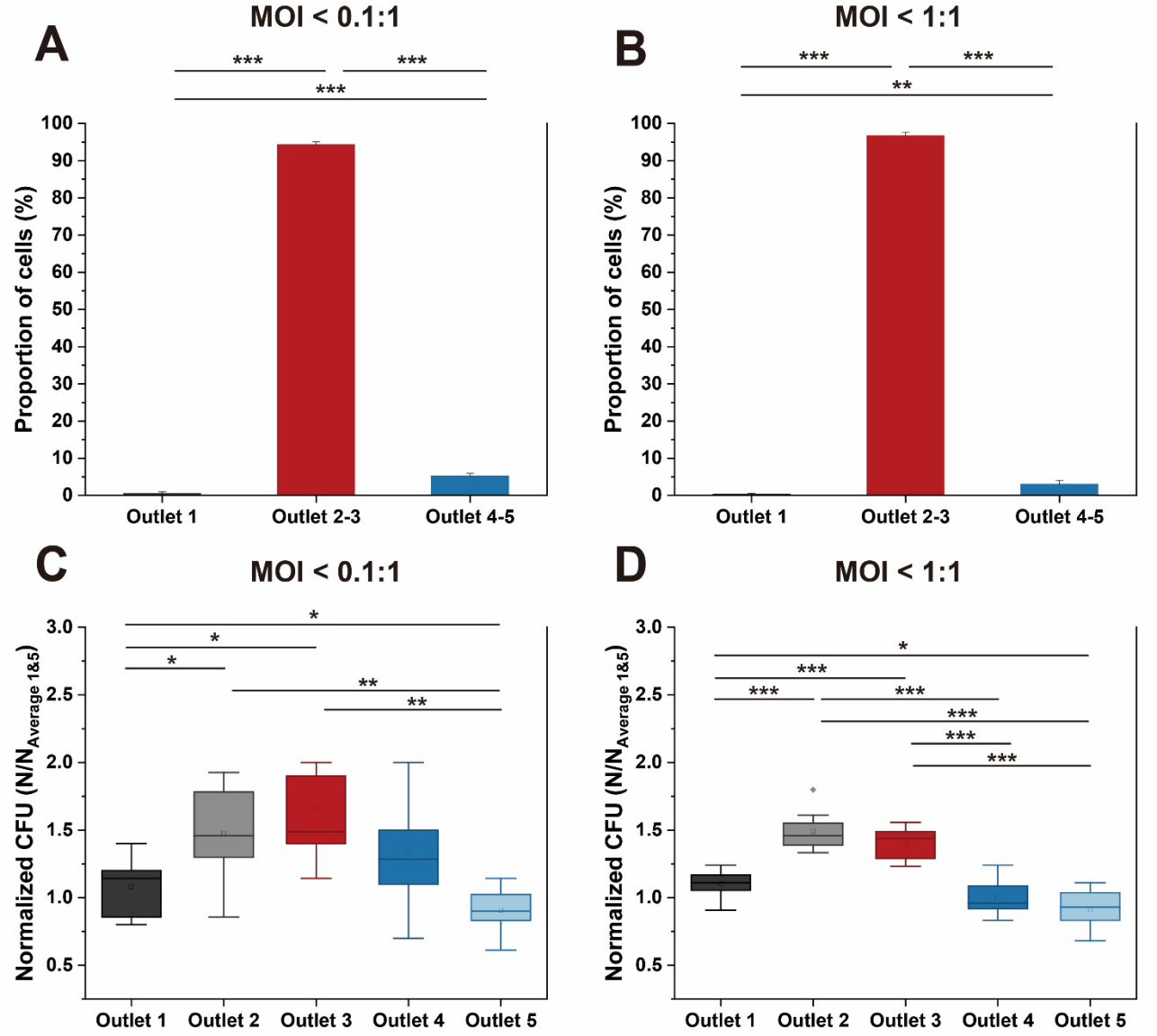

Supplementary Figure 16. The proportion of cells within target outlets for samples infected with *Streptococcus agalactiae* at A) MOI < 0.1:1, B) MOI < 1:1. Normalized CFU data in each outlet from samples infected at C) MOI < 0.1:1 and D) MOI < 1:1. CFU data were normalized to the averaged CFU of outlet 1 and 5. * states for p values of < 0.01, ** states for p values of < 0.001, *** states for p values of < 0.0001.

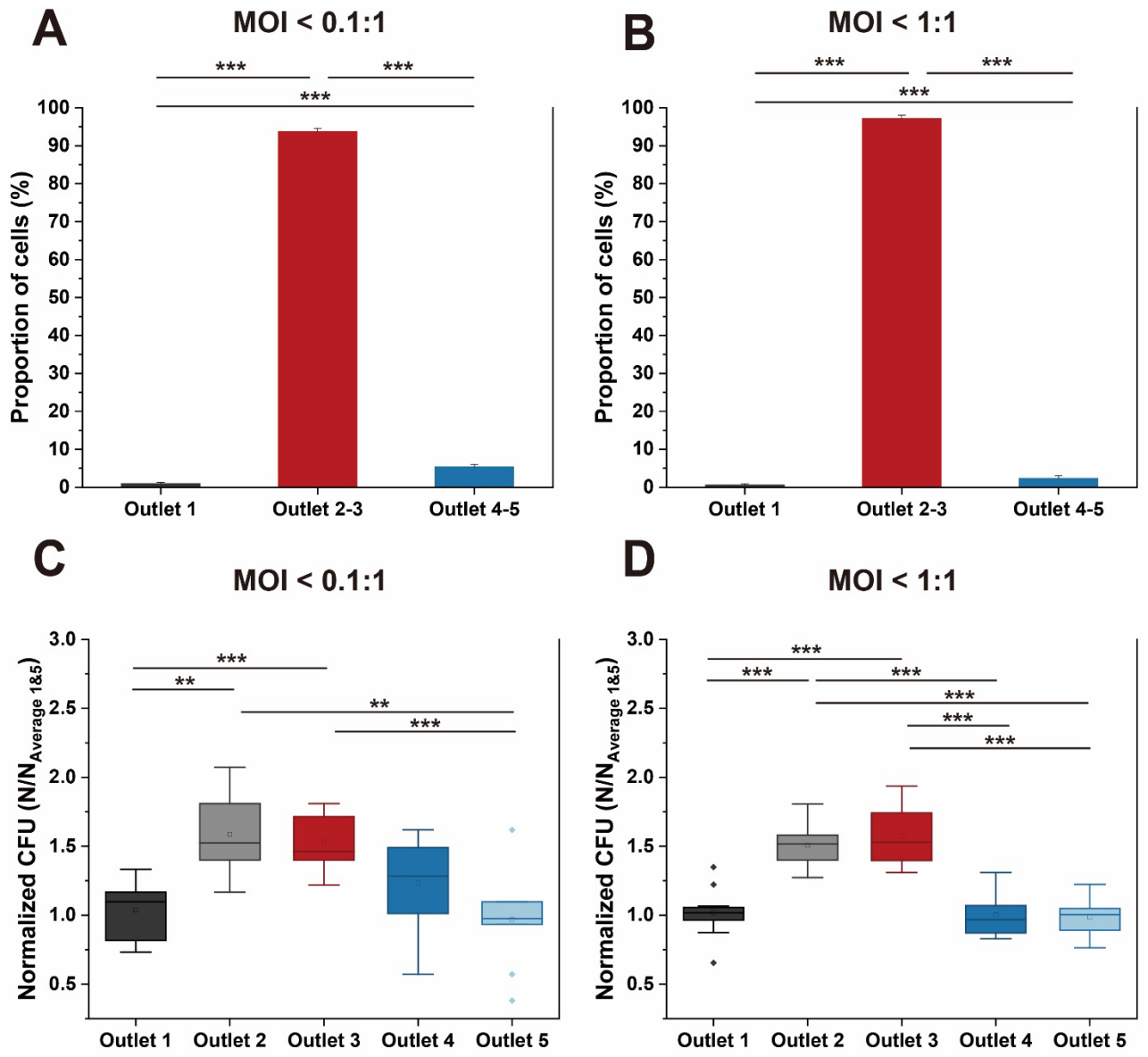

Supplementary Figure 17. The proportion of cells within target outlets for samples infected with *Klebsiella pneumonia* at A) MOI < 0.1:1, B) MOI < 1:1. Normalized CFU data in each outlet from samples infected at C) MOI < 0.1:1 and D) MOI < 1:1. CFU data were normalized to the averaged CFU of outlet 1 and 5. ** states for p values of < 0.001, *** states for p values of < 0.0001.

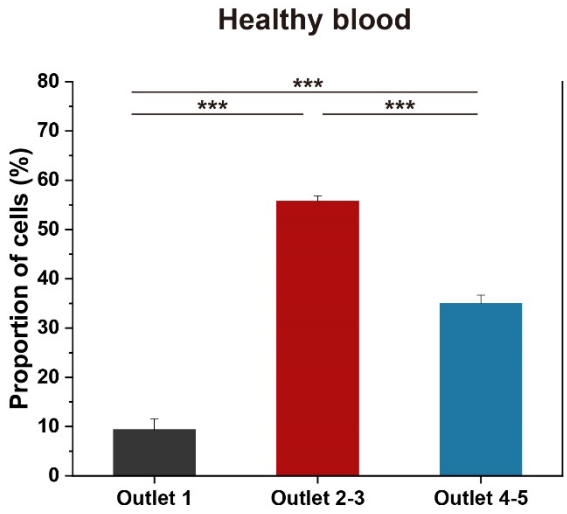

Supplementary Figure 18. Proportion of cells for healthy blood sample. *** states for p values of < 0.0001.

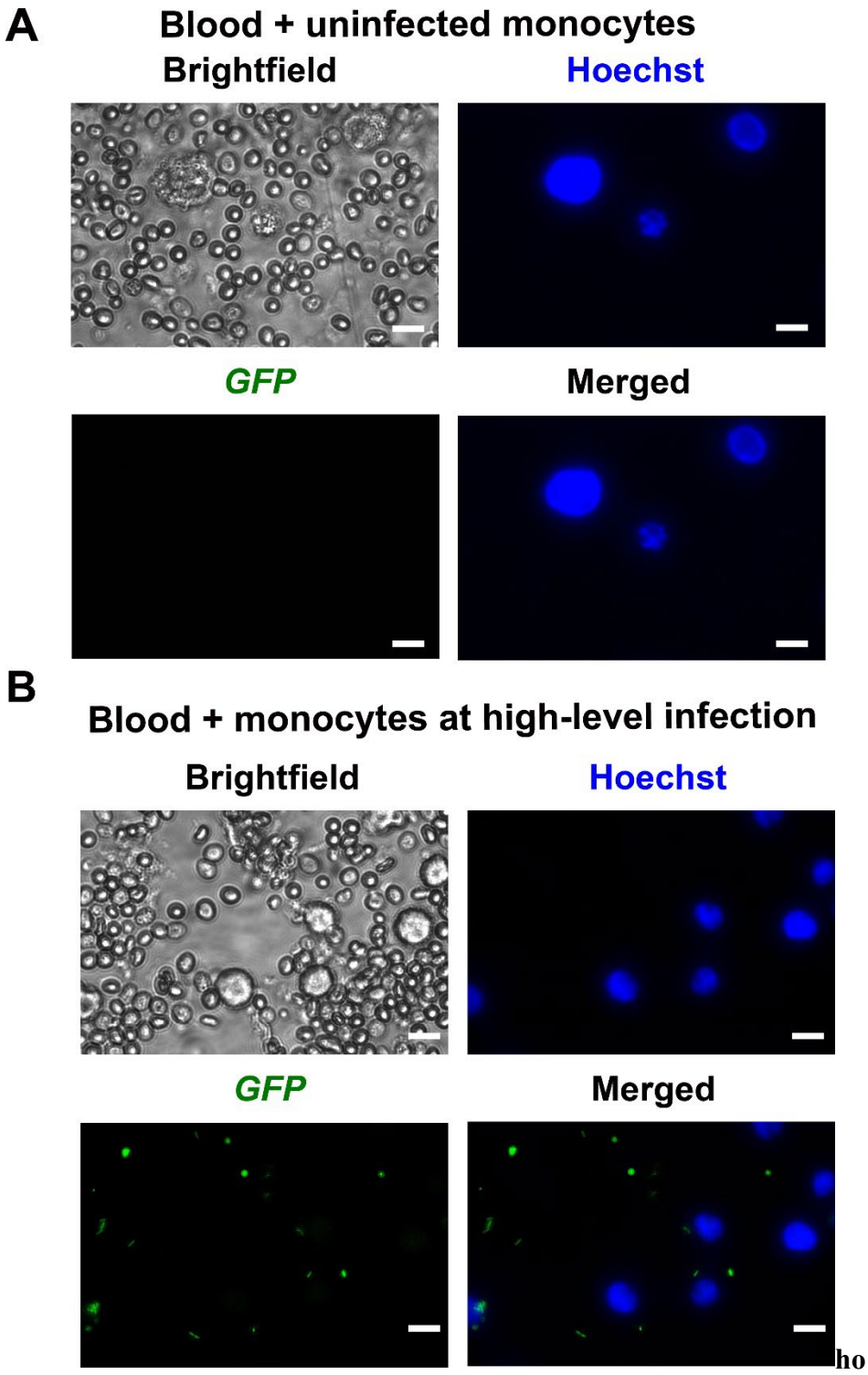

Supplementary Figure 19. Representative images of A) uninfected monocytes spiked in healthy blood samples and B) monocytes at high-level infection spiked in healthy blood samples. Scale bar = 10 μm.

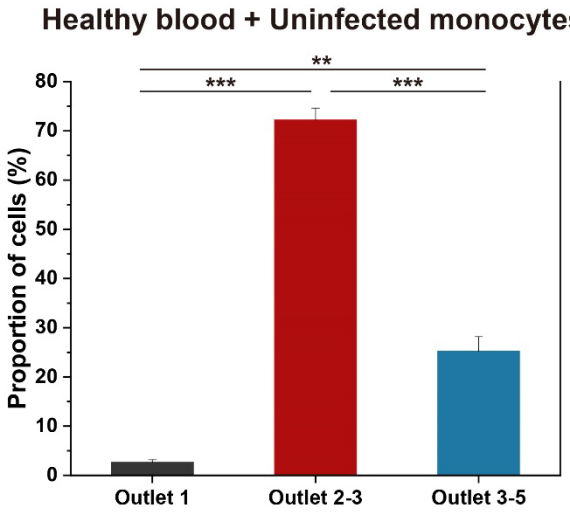

Supplementary Figure 20. Proportion of cells for blood sample spiked with uninfected monocytes. ** states for p values of < 0.001, *** states for p values of < 0.0001.

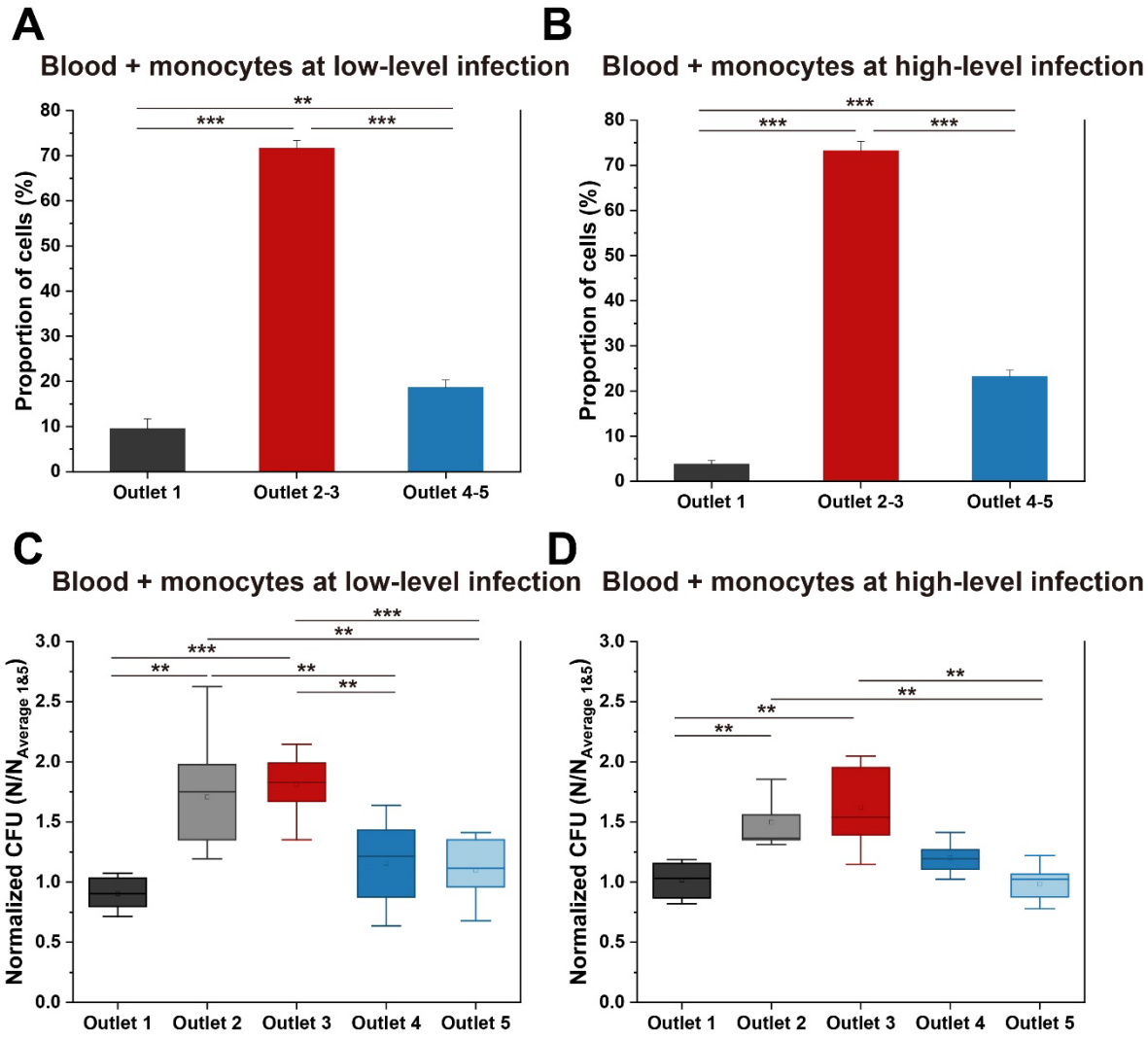

Supplementary Figure 21. The proportion of cells within target outlets for uninfected blood samples with spiked monocytes at A) low-level infection and B) high-level infection rates. Normalized CFU data in each outlet under whole blood sample spike with monocytes infected at C) low-level infection and D) high-level infection rates. CFU data were normalized to the averaged CFU of outlet 1 and 5. ** states for p values of < 0.001, *** states for p values of < 0.0001.

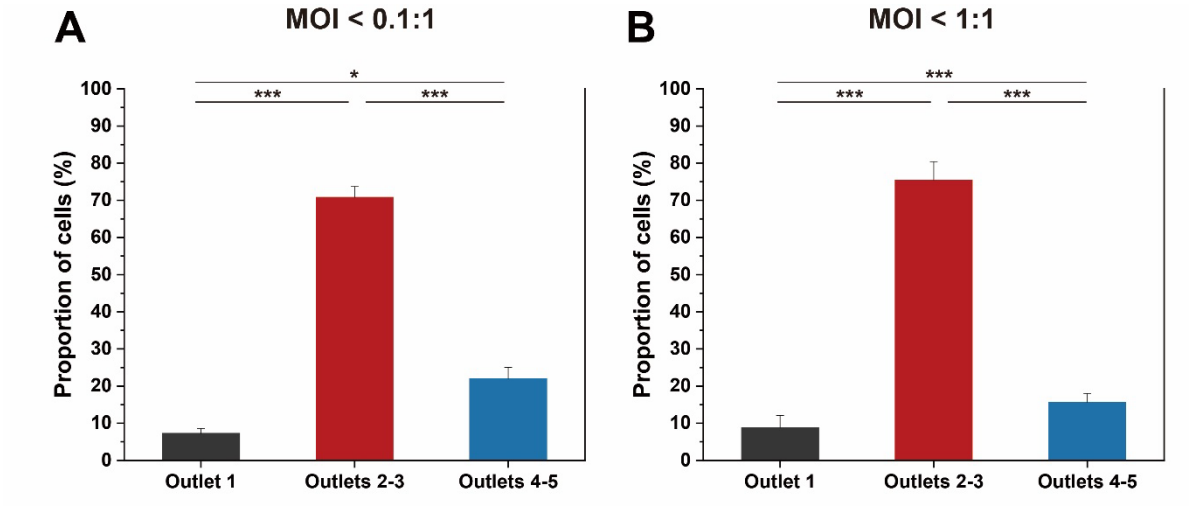

Supplementary Figure 22. The proportion of cells within target outlets for WBCs samples infected with *P. aeruginosa* at A) MOI < 0.1:1, B) MOI < 1:1. * states for p values of < 0.01, ** states for p values of < 0.001, *** states for p values of < 0.0001.

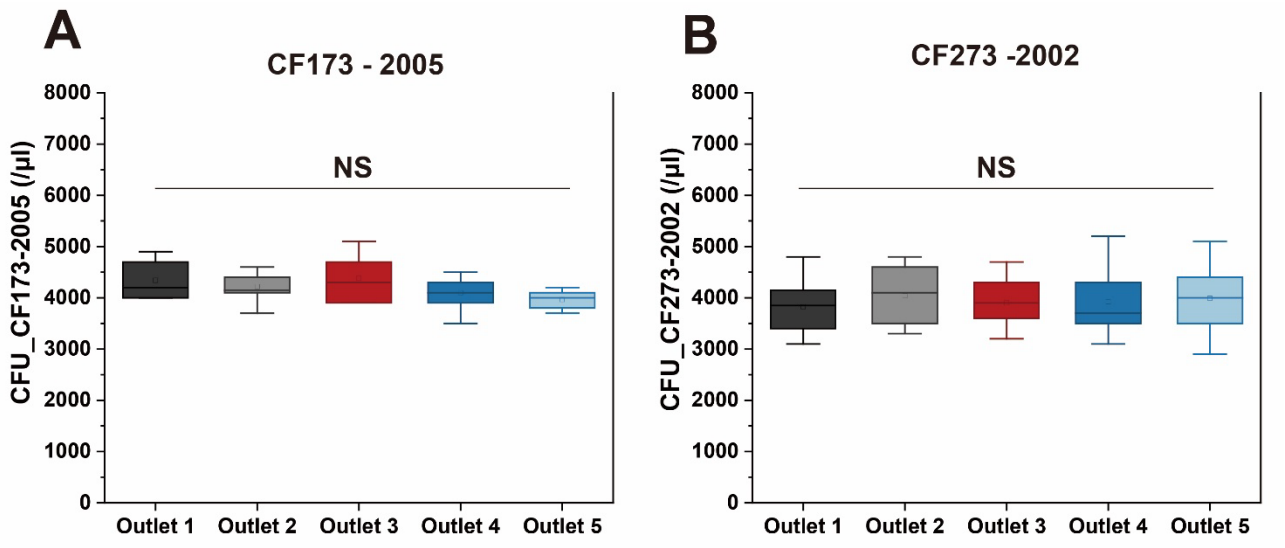

Supplementary Figure 23. Corresponding CFU counts from each outlet for samples comprising only single bacteria of A) CF173-2005 and B) CF273-2002. NS = not significant.

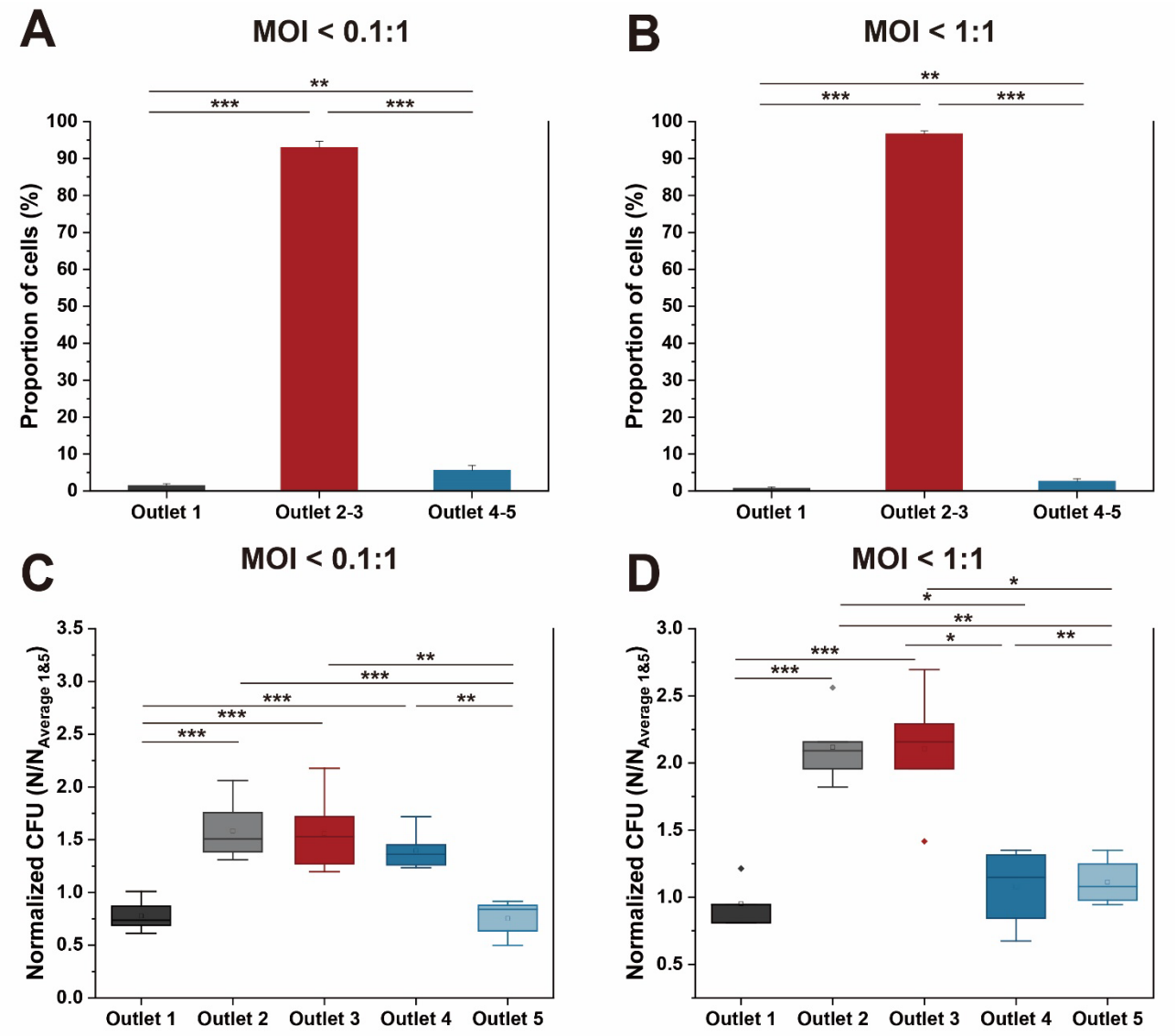

Supplementary Figure 24. The proportion of cells within target outlets for samples infected with clinical isolates CF173-2005 at A) MOI < 0.1:1, B) MOI < 1:1. Normalized CFU data in each outlet from samples infected at C) MOI < 0.1:1 and D) MOI < 1:1. CFU data were normalized to the averaged CFU of outlet 1 and 5. * states for p values of < 0.01, ** states for p values of < 0.001, *** states for p values of < 0.0001.

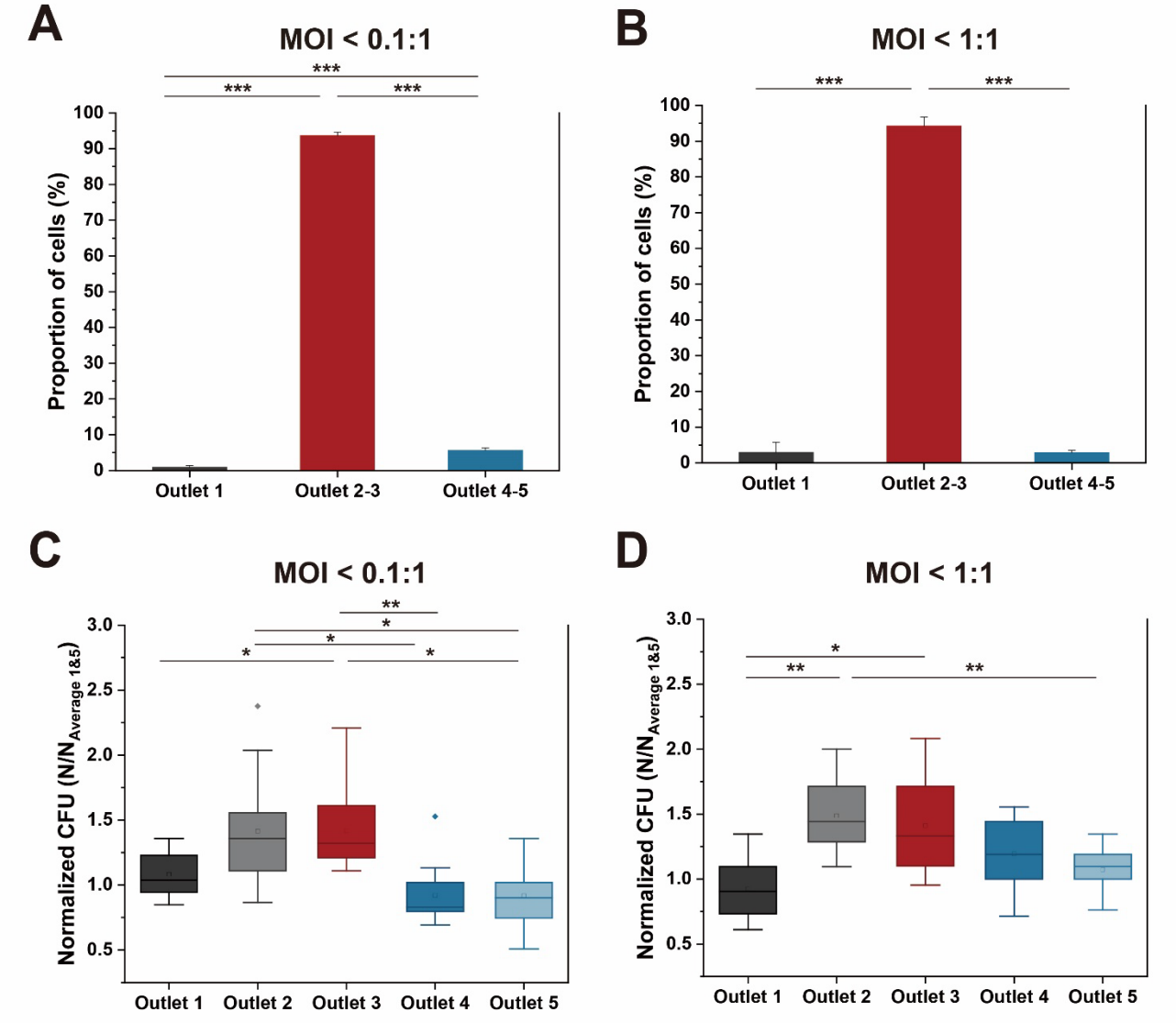

Supplementary Figure 25. The proportion of cells within target outlets for samples infected with clinical isolates CF273-2002 at A) MOI < 0.1:1, B) MOI < 1:1. Normalized CFU data in each outlet from samples infected at C) MOI < 0.1:1 and D) MOI < 1:1. CFU data were normalized to the averaged CFU of outlet 1 and 5. * states for p values of < 0.01, ** states for p values of < 0.001, *** states for p values of < 0.0001.

Acknowledgments

This study was supported by the Research Grants Council (RGC). This work was also supported by the City University of Hong Kong and the Hong Kong Polytechnic University, Environmental and Conservation Fund, and State Key Laboratory for Chemical Biology and Drug Discovery.

Funding: Research Grants Council (RGC 9610430 and 11204317); City University of Hong Kong, Hong Kong Polytechnic University (BE2B); Environmental and Conservation Fund (ECF 49/2019) and State Key Laboratory for Chemical Biology and Drug Discovery (1-BBX8).

Author contributions: Conceived and designed the experiments: BLK, SLC, JCL. Performed the experiments: JCL, JFR. Analyzed the data: BLK, SLC, JCL. Contributed reagents/materials/analysis tools: BLK, SLC, RCHW. Wrote the paper: BLK, SLC, JFR, RCHW, JCL. All authors have read the manuscript.

Competing interests: One or more authors have a pending patent related to this work.

Data and materials availability: All data needed to evaluate the conclusions in the paper are present in the paper and/or the Supplementary Materials.

References

1. Peters, R.P., et al., *New developments in the diagnosis of bloodstream infections.* The Lancet infectious diseases, 2004. **4**(12): p. 751-760.
2. Peker, N., et al., *Diagnosis of bloodstream infections from positive blood cultures and directly from blood samples: recent developments in molecular approaches.* Clin Microbiol Infect, 2018. **24**(9): p. 944-955.
3. Masters, T.A., et al., *Plasma membrane tension orchestrates membrane trafficking, cytoskeletal remodeling, and biochemical signaling during phagocytosis.* Proceedings of the National Academy of Sciences, 2013. **110**(29): p. 11875-11880.
4. Yap, B. and R.D. Kamm, *Mechanical deformation of neutrophils into narrow channels induces pseudopod projection and changes in biomechanical properties.* Journal of Applied Physiology, 2005. **98**(5): p. 1930-1939.

5. Srivastava, N., et al., *Pressure sensing through Piezo channels controls whether cells migrate with blebs or pseudopods.* Proceedings of the National Academy of Sciences, 2020. **117**(5): p. 2506-2512.
6. Buyck, J.M., P.M. Tulkens, and F. Van Bambeke, *Pharmacodynamic evaluation of the intracellular activity of antibiotics towards Pseudomonas aeruginosa PAO1 in a model of THP-1 human monocytes.* Antimicrob Agents Chemother, 2013. **57**(5): p. 2310-8.
7. Garai, P., et al., *Killing from the inside: Intracellular role of T3SS in the fate of Pseudomonas aeruginosa within macrophages revealed by mgtC and oprF mutants.* PLoS Pathog, 2019. **15**(6): p. e1007812.
8. Garcia-Medina, R., et al., *Pseudomonas aeruginosa Acquires Biofilm-Like Properties within Airway Epithelial Cells.* Infection and Immunity, 2005. **73**(12): p. 8298-8305.
9. Hu, S., et al., *Revealing elasticity of largely deformed cells flowing along confining microchannels.* RSC advances, 2018. **8**(2): p. 1030-1038.
10. Bedi, B., et al., *Enhanced Clearance of Pseudomonas aeruginosa by Peroxisome Proliferator-Activated Receptor Gamma.* Infect Immun, 2016. **84**(7): p. 1975-1985.
11. Shin, H., et al., *Pseudomonas aeruginosa GroEL Stimulates Production of PTX3 by Activating the NF-kappaB Pathway and Simultaneously Downregulating MicroRNA-9.* Infect Immun, 2017. **85**(3).
12. Zhou, Y., Z. Ma, and Y. Ai, *Sheathless inertial cell focusing and sorting with serial reverse wavy channel structures.* Microsyst Nanoeng, 2018. **4**: p. 5.
13. Herrmann, N., P. Neubauer, and M. Birkholz, *Spiral microfluidic devices for cell separation and sorting in bioprocesses.* Biomicrofluidics, 2019. **13**(6): p. 061501.
14. Chen, C.K. and B.L. Khoo, *A density-based threshold model for evaluating the separation of particles in heterogeneous mixtures with curvilinear microfluidic channels.* Sci Rep, 2020. **10**(1): p. 18984.
15. Khoo, B.L., et al., *Liquid biopsy for minimal residual disease detection in leukemia using a portable blast cell biochip.* NPJ Precis Oncol, 2019. **3**: p. 30.
16. Lim, E.J., et al., *Inertio-elastic focusing of bioparticles in microchannels at high throughput.* Nat Commun, 2014. **5**: p. 4120.
17. Amini, H., W. Lee, and D. Di Carlo, *Inertial microfluidic physics.* Lab Chip, 2014. **14**(15): p. 2739-61.
18. Guzniczak, E., et al., *Deformability-induced lift force in spiral microchannels for cell separation.* Lab on a Chip, 2020. **20**(3): p. 614-625.
19. Gossett, D.R., et al., *Hydrodynamic stretching of single cells for large population mechanical phenotyping.* Proc Natl Acad Sci U S A, 2012. **109**(20): p. 7630-5.
20. Amini, H., W. Lee, and D. Di Carlo, *Inertial microfluidic physics.* Lab on a Chip, 2014. **14**(15): p. 2739-2761.
21. Mok, N., et al., *Vanillin inhibits PqsR-mediated virulence in Pseudomonas aeruginosa.* Food & Function, 2020. **11**(7): p. 6496-6508.
22. Francis, M.S. and C.J. Thomas, *Effect of multiplicity of infection on Listeria monocytogenes pathogenicity for HeLa and Caco-2 cell lines.* J Med Microbiol, 1996. **45**(5): p. 323-30.
23. Chua, S.L., et al., *Reactive oxygen species drive evolution of pro-biofilm variants in pathogens by modulating cyclic-di-GMP levels.* Open Biology, 2016. **6**(11): p. 160162.
24. Orsini, J., et al., *Microbiological profile of organisms causing bloodstream infection in critically ill patients.* Journal of clinical medicine research, 2012. **4**(6): p. 371.
25. Rosales, C., *Neutrophil: a cell with many roles in inflammation or several cell types?* Frontiers in physiology, 2018. **9**: p. 113.
26. Dean, L. and L. Dean, *Blood groups and red cell antigens*. Vol. 2. 2005: NCBI Bethesda, Md, USA.

27. Mickiewicz, K.M., et al., *Possible role of L-form switching in recurrent urinary tract infection.* Nat Commun, 2019. **10**(1): p. 4379.
28. Tuchscherr, L., et al., *Staphylococcus aureus phenotype switching: an effective bacterial strategy to escape host immune response and establish a chronic infection.* EMBO Mol Med, 2011. **3**(3): p. 129-41.
29. Lee, A., et al., *Detection of bloodstream infections in adults: how many blood cultures are needed?* J Clin Microbiol, 2007. **45**(11): p. 3546-8.
30. Chua, S.L., et al., *Selective labelling and eradication of antibiotic-tolerant bacterial populations in Pseudomonas aeruginosa biofilms.* Nature communications, 2016. **7**(1): p. 1-11.
31. Yang, L., et al., *Evolutionary dynamics of bacteria in a human host environment.* Proceedings of the National Academy of Sciences, 2011. **108**(18): p. 7481-7486.
32. Chua, S.L., et al., *Dispersed cells represent a distinct stage in the transition from bacterial biofilm to planktonic lifestyles.* Nature Communications, 2014. **5**(1): p. 4462.
33. Hu, S., et al., *Multiparametric biomechanical and biochemical phenotypic profiling of single cancer cells using an elasticity microcytometer.* small, 2016. **12**(17): p. 2300-2311.
34. Ren, J., et al., *Nondestructive quantification of single-cell nuclear and cytoplasmic mechanical properties based on large whole-cell deformation.* Lab on a Chip, 2020. **20**(22): p. 4175-4185.
35. Chan, S.Y., et al., *Biofilm matrix disrupts nematode motility and predatory behavior.* The ISME Journal, 2020.
36. Blauwkamp, T.A., et al., *Analytical and clinical validation of a microbial cell-free DNA sequencing test for infectious disease.* Nature microbiology, 2019. **4**(4): p. 663-674.
37. Shen, H., et al., *Rapid and Selective Detection of Pathogenic Bacteria in Bloodstream Infections with Aptamer-Based Recognition.* ACS Appl Mater Interfaces, 2016. **8**(30): p. 19371-8.
38. Zhu, Y., et al., *Sensitive and fast identification of bacteria in blood samples by immunoaffinity mass spectrometry for quick BSI diagnosis.* Chem Sci, 2016. **7**(5): p. 2987-2995.
39. Conzelmann, C., et al., *An enzyme-based immunodetection assay to quantify SARS-CoV-2 infection.* Antiviral Res, 2020. **181**: p. 104882.
40. Kang, D.K., et al., *Rapid detection of single bacteria in unprocessed blood using Integrated Comprehensive Droplet Digital Detection.* Nat Commun, 2014. **5**: p. 5427.